UNIVERSITEIT VAN PRETORIA
UNIVERSITY OF PRETORIA
YUNIBESITHI YA PRETORIA

Longitudinal vehicle dynamics control for improved vehicle safety

by

Herman Adendorff Hamersma

Submitted in partial fulfilment of the requirements for the degree

Master of Engineering (Mechanical Engineering)

in the

Faculty of Engineering, Built Environment and Information Technology (EBIT)

University of Pretoria

September 2013

Summary

Title: Longitudinal vehicle dynamics control for improved vehicle safety

Author: Herman Adendorff Hamersma

Supervisor: Prof P.S. Els

Department: Mechanical and Aeronautical Engineering, University of Pretoria

Degree: Master of Engineering (Mechanical Engineering)

An autonomous vehicle is a vehicle that is capable of navigating and driving with no human intervention whatsoever through the utilization of various sensors and positioning systems. The possible applications of autonomous vehicles are widespread, ranging from the aerospace industry to the mining and military sectors where the exposure of human operators to the operating conditions is hazardous to their health and safety. Automobile accidents have become the leading cause of death in certain segments of the world population. Removing the human driver from the decision-making process through automation may result in significantly safer highways. Although full autonomy may be the ultimate goal, there is huge scope for systems that aid the driver in decision making or systems that take over from the driver under conditions where the human driver fails.

The aim of the longitudinal control system to be implemented on the Land Rover test vehicle in this study is to improve the vehicle's safety by controlling the vehicle's longitudinal behaviour. A common problem with sports-utility-vehicles is the low rollover threshold, due to a high centre of gravity. Rather than modifying the vehicle to increase the rollover threshold, the aim of the control system presented here is to prevent the vehicle from exceeding speeds that would cause the vehicle to reach its rollover threshold.

In order to develop a control system that autonomously controls the longitudinal degree of freedom, a model of the test vehicle (a 1997 Land Rover Defender 110 Wagon) was developed in MSC.ADAMS/View and validated experimentally. The model accurately captures the response of the test vehicle to supply forces as generated by the engine and demand forces applied through drag, braking and engine braking. Furthermore, the model has been validated experimentally to provide reliable simulation results for lateral and vertical dynamics.

The control system was developed by generating a reference speed that the vehicle must track. This reference speed was formulated by taking into account the vehicle's limits due to lateral acceleration, combined lateral and longitudinal acceleration and the vehicle's performance

capabilities. The control system generates the desired throttle pedal position, hydraulic pressure in the brake lines, clutch position and gear selection as output. The MSC.ADAMS\View model of the test vehicle was used to evaluate the performance of the control system on various racetracks of which the GPS coordinates were available. The simulation results indicate that the control system performs as expected.

Finally, the control system was implemented on the test vehicle and the performance was evaluated by conducting field tests in the form of a severe double lane change manoeuvre. The results of the field tests indicated that the control system limited the acceleration vector of the vehicle's centre of gravity to prescribed limits, as predicted by the simulation results.

Acknowledgements

I would like to extend my gratitude towards the following people, without whom successful completion of this project would not have been possible:

- Prof Schalk Els, for his friendship, mentorship and guidance throughout my studies.
- My wife Anneke, for her unconditional love, support, understanding and acceptance.
- My mother Susan and grandparents Kris and Riekie, for their advice and unwavering support.
- My brother Kristian, for his unique perspective.
- Theunis Botha, for his willingness to share his vast knowledge of the Land Rover and the systems implemented on it.
- The Vehicle Dynamics Group at the University of Pretoria, for their eagerness to help whenever extra hands were required.

Table of Contents

List of Figures

List of Tables

List of Symbols

Lowercase Roman symbols

Symbol	Description	Unit
c_i	Constant term of straight line describing perpendicular bisector	[m]
d_{prev}	Preview distance	[m]
e	Velocity error	[m/s]
g	Gravitational acceleration	[m/s^2]
h	Height of centre of gravity	[m]
i	Index	[Dimensionless]
$\hat{\boldsymbol{\imath}}$	Unit vector in x-direction	[Dimensionless]
$\hat{\boldsymbol{\jmath}}$	Unit vector in y-direction	[Dimensionless]
m_i	Gradient of chord of ith segment of trajectory	[Dimensionless]
m'_i	Gradient of perpendicular bisector of chord of ith segment of trajectory	[Dimensionless]
n	Engine speed	[RPM]
n_{seg}	Number of track segments	[Dimensionless]
p_{00} - p_{40}	Coefficients of three dimensional polynomial	[Dimensionless]
r	Free variable used for parameterisation of curves	[Dimensionless]
s	Arc length	[m]
Δs_i	Length of ith track segment	[m]
t	Time	[s]
t_w	Vehicle track width	[m]
u	PID controller input	[Dimensionless]
x	Coordinate x value	[m]
x_l	Left edge (bound) of road's x-coordinate	[m]
$x_{q,i}$	X-coordinate of centre point of chord of ith segment of trajectory	[m]
x_r	Right edge (bound) of road's x-coordinate	[m]
$x_{R,i}$	X-coordinate of centre point of arc of of ith segment of trajectory	[m]
Δx_i	Change in x-distance of ith track segment	[m]
y	Coordinate y value	[m]
y_l	Left edge (bound) of road's y-coordinate	[m]
$y_{q,i}$	Y-coordinate of centre point of chord of ith segment of trajectory	[m]
y_r	Right edge (bound) of road's y-coordinate	[m]
$y_{R,i}$	Y-coordinate of centre point of arc of of ith segment of trajectory	[m]
Δy_i	Change in y-distance of ith track segment	[m]

Uppercase Roman symbols

Symbol	Description	Unit
A_f	Projected frontal area	[m^2]
A_{Brakes}	Acceleration due to braking	[m/s^2]
A_x	Acceleration in the x-direction (longitudinal)	[m/s^2]
A_y	Acceleration in the y-direction (lateral)	[m/s^2]
B_s	Linear coefficient matrix of quadratic cost function for shortest distance formulation	[Dimensionless]
B_κ	Linear coefficient matrix of quadratic cost function for minimum curvature formulation	[Dimensionless]
C_D	Aerodynamic drag coefficient	[Dimensionless]
F_{Brakes}	Braking force	[N]
F_{Incl}	Component of gravity due to inclination	[N]
F_D	Demand force	[N]
F_{Drag}	Aerodynamic drag force	[N]
F_{rr}	Rolling resistance force	[N]
F_y	Lateral (cornering) force	[N]
F_{yf}	Lateral force at the front wheels	[N]
F_{yr}	Lateral force at the rear wheels	[N]
H_s	Hessian matrix of quadratic cost function for shortest distance formulation	[Dimensionless]
H_κ	Hessian matrix of quadratic cost function for minimum curvature formulation	[Dimensionless]
K_D	PID derivative gain	[Dimensionless]
K_I	PID integral gain	[Dimensionless]
K_P	PID proportional gain	[Dimensionless]
M	Mass of vehicle	[kg]
P	Position of vehicle on road	[m]
P_{hyd}	Brake line hydraulic pressure	[bar]
ΔP_i	Distance between consecutive road positions	[m]
ΔP_x	Distance between x-coordinates of consecutive road positions	[m]
ΔP_y	Distance between y-coordinates of consecutive road positions	[m]
R	Radius of turn	[m]
R_{RR}	Rolling radius	[m]
S	Distance	[m]
T	Throttle position	[%]
T_{Engine}	Engine torque	[Nm]
T_{EBT}	Engine braking torque	[Nm]
V	Velocity	[m/s]
V_{ref}	Reference velocity	[m/s]

Greek symbols

Symbol	Description	Unit
α	Parameter identifying position of vehicle on the road between the boundaries	[Dimensionless]
α_s	Parameter identifying position of vehicle on the road for shortest distance formulation	[Dimensionless]
α_κ	Parameter identifying position of vehicle on the road for minimum curvature formulation	[Dimensionless]
$\dot{\delta}_{\psi,FFNN}$	Feed Forward Neural Network controller steer rate output	[rad/s]
θ	Longitudinal vehicle inclination	[Radians]
κ	Curvature of trajectory	[Dimensionless]
λ	Longitudinal tyre slip	[%]
μ	Friction coefficient	[Dimensionless]
μ_{rr}	Coefficient of rolling resistance	[Dimensionless]
ρ	Density of air	[kg/m^3]
τ	Preview time	[s]
ψ	Yaw angle	[rad]
$\dot{\psi}$	Yaw rate	[rad/s]
$\ddot{\psi}$	Yaw acceleration	[rad/s^2]
ψ_d	Desired yaw angle	[rad]
ψ_0	Vehicle's current yaw angle	[rad]
ω	Wheel rotational speed	[rad]

Chapter 1

Introduction and literature survey

Besides black art, there is only automation and mechanization

- Federico Garcia Lorca (1898-1936) Spanish poet

1.1 Introduction

Automation is the buzzword in modern engineering and has been applied extensively in the field of vehicle engineering. Applications of automation in vehicle engineering range from rain sensing windscreen wipers to climate control systems. More specific to the study of vehicle dynamics is the improvement achievable by implementing feedback control systems which influence the dynamic behaviour of the vehicle with regards to the six degrees of freedom, namely lateral, vertical and longitudinal translation as well as roll, pitch and yaw rotation. Application of automation to control these degrees of freedom may lead to the optimisation of vehicle utilisation.

An autonomous vehicle is a vehicle that is capable of navigating and driving with no human intervention whatsoever through the utilisation of various sensors and positioning systems. The possible applications for autonomous vehicles are widespread, ranging from the aerospace industry to the mining and military sectors where the exposure of human operators to the harsh operating conditions is hazardous to their health and safety. Recently, there have been several initiatives promoting research into the field of autonomous vehicles, specifically in 2001 when the United States National Defence Authorization Act mandated that:

> "*It shall be a goal of the Armed Forces to achieve the fielding of unmanned, remotely controlled technology such that… by 2015, one-third of the operational ground combat vehicles are unmanned.*" (DARPA, 2008).

The Defence Advanced Research Project Agency (DARPA) conducted the Urban Challenge and Grand Challenge programs in support of this Congressional mandate. These challenges are best described as a field test of autonomous ground vehicles over realistic terrain. A large focus of the DARPA challenges were on the Artificial Intelligence (AI) implemented on the vehicles, but the vehicle dynamics (in comparison to the AI) were largely neglected. Currently, there are several projects at the University of Pretoria aimed at converting a standard 1997 Land Rover Defender

300 Tdi (see Figure 1.1) to an autonomous vehicle which, if successful, will provide a platform for implementing such AI systems while operating the vehicle at optimum performance.

Applying automation to the guidance of ground vehicles may have the benefit of improving highway safety. Advanced Vehicle Control Systems (AVCS) are part of the "Smart Highway" initiative (also known as the Intelligent Vehicle Highway System (IVHS)) and is the topic of extensive research worldwide (Goldsmith, 1998). According to Goldsmith (1998), automobile accidents have become the leading cause of death in certain segments of the American population. The World Health Organization has identified road traffic injuries as the leading cause of death by injury, the 10th leading cause of all deaths and the 9th leading contributor to the burden of disease worldwide (Peden *et al.,* 2002). Assisting or even removing the human driver from the decision-making process through automation may result in significantly safer highways and serves as further motivation for the extensive research into the automation of automobiles.

Implemented on the University of Pretoria's Land Rover test vehicle are feedback control systems that can mimic the inputs given by a human driver. These feedback control systems have been implemented in such a way that the Land Rover test vehicle may be driven manually or via a computer. Several driver assist systems that lie somewhere between no control and fully autonomous control, such as an Anti-Lock Braking System (ABS) and Traction Control, can be implemented on the Land Rover test vehicle. The systems implemented on the vehicle consist of (more detail in the next section):

- a path following steering control system capable of fully autonomous control up to high lateral acceleration limits
- a braking control system
- a gear-shift and clutch control system
- a throttle pedal control system

The development of these control systems resulted from various undergraduate, honours and masters' degree projects over the past five years. These systems are described in more detail in Chapter 2.

Figure 1.1 – The Land Rover Defender test vehicle

1.2 Literature survey

1.2.1 Existing autonomous vehicles

There are several projects worldwide aimed at developing autonomous vehicles, of which the most famous are probably the Google autonomous car (Technology Talks, 2010) and the DARPA Urban and Desert Grand Challenges (Montemerlo *et al.* 2006) that were organised by the US Government to foster research and development in the field of autonomous driving.

The 2005 DARPA Desert Grand Challenge was won by the Stanford Racing Team (Montemerlo *et al.* 2006) with their autonomous vehicle, named Stanley. Stanley finished the DARPA Grand Challenge in 6 hours, 53 minutes and 58 seconds at an average speed of 19.1 miles per hour (30.7 kilometres per hour). The vehicle was steered with a steering controller that used inputs from various modules, including a Global Positioning System (GPS) and lasers and a camera for obstacle detection and vision mapping. The velocity control of the vehicle also incorporated numerous constraints to determine the desired velocity of the vehicle, such as the dynamic constraints on maximum lateral accelerations as well as the terrain slope, the distance from obstacles and the roughness of the terrain (Montemerlo *et al.*, 2006). Figure 1.2 (Montemerlo *et al.,* 2006) shows Stanley as used in the 2005 DARPA Grand Challenge.

Figure 1.2 – Stanley, Stanford Racing Team's DARPA entry (Montemerlo *et al.,* 2006)

In 2010, Google announced that it had produced a fleet of driverless Toyota Prius vehicles, having driven more than 225 000km autonomously. According to Google, the vehicle uses virtual images created by the vehicle's software from inputs from radar sensors, a LIDAR (Light Detection And Ranging) sensor, a position sensor which locates the vehicle's position on a map and video cameras. (Technology Talks: 2010). However, very little technical information is available on the Google autonomous car, peer reviewed articles have not been published on the subject.

The use of autonomous control systems as driver assist systems are also becoming prevalent in the commercial market. Intelligent parking assist systems mainly use vision-based control systems to determine the path the vehicle has to follow (Vestri *et al.,* 2005). These intelligent parking assist systems still rely on the driver to operate the throttle and brake and are performed at very low speeds.

Another interesting topic in the field of autonomous vehicle development is the application of platooning or vehicle following. Ioannou and Chien (1993) developed an autonomous intelligent cruise control system for automatic vehicle following and examined its effect on traffic flow. The control system developed did not rely on vehicle to vehicle communication, rather relying on a safe following distance dependent on vehicle speed. Although their work was limited to simulation models and not implemented experimentally, similar technology has become readily available in the commercial automotive market. Notably Volvo, Infiniti and Mercedes-Benz have implemented vehicle following systems and similar systems are now available on numerous other car manufacturers ('Tech Inside: Autonomous Emergency Braking', 2012). These autonomous intelligent cruise control systems are sometimes referred to as adaptive cruise controls and are intended as driver assist systems that are able to regulate speed and following distance. The adaptive cruise control systems enable driving at shorter following distances and higher speeds, while providing smoother acceleration and deceleration. This contributes to a more stable traffic flow (Hoedemaeker *et al*, 1998).

1.2.2 Vehicle Dynamics

The main research topic being addressed by the Vehicle Dynamics Group (VDG) at the University of Pretoria is to improve the understanding of the dynamics associated with ground vehicles and to use this understanding of vehicle dynamics to optimise ground vehicle design (be it through mathematical modelling and simulation or automation) with the application of modern engineering techniques.

Gillespie (1992: 5) repeats the familiar saying that the primary forces acting on a ground vehicle (excluding the aerodynamic forces) that are used to control its dynamic behaviour are developed in the tyre contact patches, each approximately the size of a male human hand for a typical passenger vehicle. When controlling a vehicle, the driver exercises control over these forces through his/her inputs to the various controls at his/her disposal. Blundell and Harty (2004: 399) state that the main factors which influence the driver's actions are speed and path. Speed is controlled by engine power (through throttle position and gear selection) and the braking system. The path being followed by the vehicle at a given speed is controlled with the steering wheel, which is often referred to as a yaw rate demand. Combining the yaw rate with the forward velocity vector (due to the vehicle speed) gives rise to a curved path or trajectory being followed by the vehicle.

Before launching into an extensive analogy on the important aspects of vehicle dynamics, it is important to define the axis system to be used throughout this project. The Society of Automotive Engineers (SAE) defined the axis system shown in Figure 1.3 (Jazar 2008: 99). The x-axis is the intersection of the tyre plane and the road, with the positive direction being forward and is often referred to as the longitudinal direction. The z-axis is perpendicular to the road plane, with the positive direction downward. The y-axis is in the road plane, with its direction chosen to make the coordinate system orthogonal and right-hand (Gillespie 1992: 338), i.e. positive to the right. The y-axis is often referred to as the lateral direction.

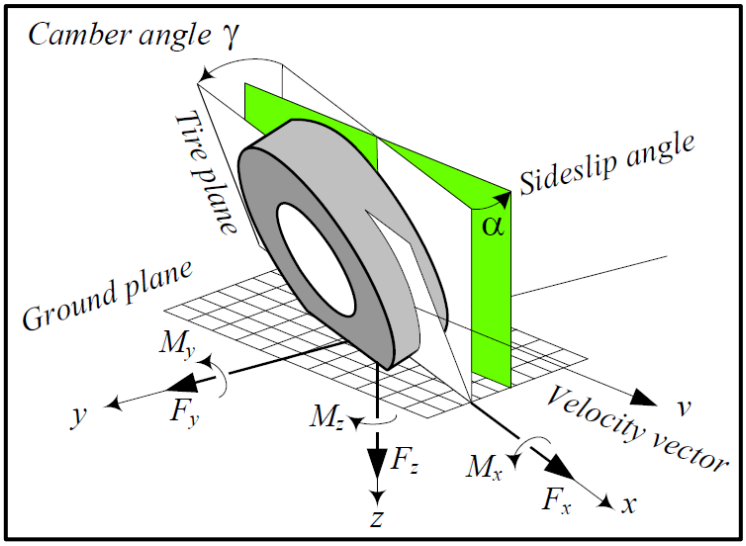

Figure 1.3 – SAE axis system (Jazar 2008: 99)

1.2.2.1 Longitudinal vehicle dynamics

Longitudinal vehicle forces may be divided into two categories, namely supply and demand forces. Supply forces are all forces that are controlled by the driver in the longitudinal direction and the demand forces are all the forces that oppose this motion. The supply forces are generated by the engine that are then transmitted to the wheels and act on the ground via the power train and by the brakes that decelerate the vehicle. The engine is typically characterised by its torque and power curves as a function of engine speed (Gillespie 1992: 21-22).

The demand forces acting on the vehicle are due to aerodynamic drag, tyre rolling resistance and the component of gravity acting in the longitudinal direction due to an inclination in the road. The Equation governing the demand forces is given by Gillespie (1992: 45-123):

$$F_D = -F_{Drag} - F_{rr} - F_{Incl} \qquad (1.1)$$
$$= -{}^1\!/_2\,\rho V^2 C_D A_f - \mu_{rr} M g \cos\theta - M g \sin\theta$$

1.2.2.2 Tyres

The main control forces that determine how a vehicle turns, brakes and accelerates (apart from the aerodynamic loads) are developed at the tyre-road interface known as the contact patch (Gillespie 1992: 335). A proper understanding of the mechanism of force and moment generation of the contact patch is thus extremely important to the engineer aiming to control a road vehicle autonomously. According to Gillespie (1992: 335), a tyre has three basic functions:

- supporting the vertical load
- developing longitudinal forces
- developing lateral forces.

Prior to discussing the mechanism of force generation, it is important to define longitudinal and lateral slip of the tyre, as these are the independent variables that longitudinal and lateral forces are usually characterised against. Longitudinal slip is defined by Gillespie (1992: 343) as a percentage of the forward speed as:

$$\lambda = \left(1 - \frac{R_{RR}\omega}{V}\right) \times 100\% \qquad (1.2)$$

The lateral slip, or side slip angle, is defined by Gillespie (1992: 348) as the difference between the direction of tyre heading and the direction the vehicle is travelling in. This is shown in Figure 1.3 and is usually denoted by the symbol α.

The forces developed on a tyre and by the tyre are not applied to a point, but result from normal and shear stresses distributed in the contact patch (Gillespie 1992: 340). A tyre rolling on a road develops both lateral and longitudinal forces by a shear mechanism – each element of the tyre tread passing through the contact patch exerts a shear stress (Gillespie 1992: 341).

There are two primary mechanisms of force coupling between the road and the tyre, namely friction (or adhesion) and hysteresis. The intermolecular bonds between the rubber and the road surface lead to the adhesion mechanism of force generation. The adhesion mechanism is greatly influenced by the driving conditions (i.e. wet or dry) – this accounts for the loss of grip on wet roads. The hysteresis mechanism of force generation arises due to the energy loss in the rubber when it deforms over the road surface. The driving conditions do not influence the hysteresis mechanism as significantly as it influences the adhesion mechanism. A final note with regard to the friction generation mechanism is that the amount of slip significantly influences the friction generated (for both adhesion and hysteresis mechanisms) (Gillespie 1992: 341-342). As the tread elements come into contact with the road surface they cannot develop a friction force due to their compliance, some bending of the elements (or slip) is required. As the tread elements progress through the contact patch the deflection is increased and hence the friction force is increased. Since a difference in the tyre's rolling speed and speed of travel is required to facilitate this bending, slip is present in the contact patch (Gillespie 1992: 343). Figure 1.4 shows a plot of lateral force as a function of side-slip angle (lateral slip) as used in this study.

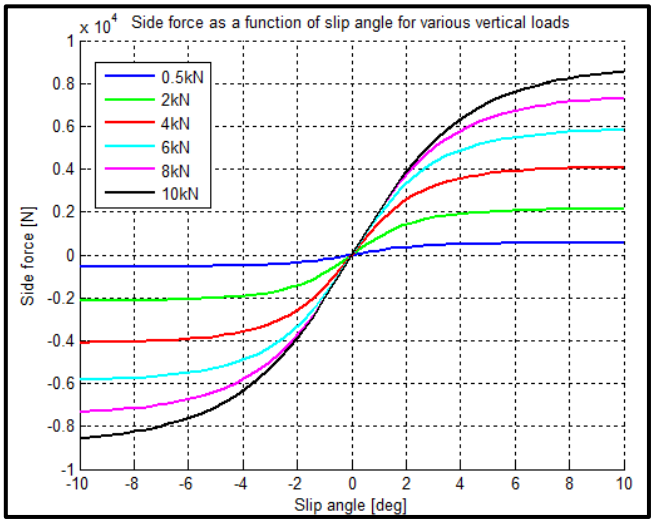

Figure 1.4 – Lateral force as a function of side-slip angle for various vertical loads

When exposing a tyre to simultaneous cornering and braking (i.e. simultaneous longitudinal and lateral force generation), it is noted that the forces developed depart significantly from the forces developed when operating the tyre under independent lateral and longitudinal slip conditions. It is observed that, as the brake force is increased, the lateral force developed diminishes (see Figure 1.5). This gives rise to the concept known as the friction circle (Gillespie 1992: 363-364). The friction circle (a plot of lateral force as a function of longitudinal force at various constant slip angles) is given in Figure 1.5. Gillespie (1992: 364) summarizes the concept of the friction circle by highlighting the fact that the maximum force that may be generated by a tyre in any direction is determined by the peak coefficient of friction and the vertical load applied to the tyre. It may therefore be assumed that the magnitude of the vector sum of the lateral and longitudinal forces cannot exceed the friction limit, hence the limit being characterized by a circle on the plot of lateral force as a function of longitudinal force. In some cases friction circle is actually an ellipse due to tyre construction and asymmetric tread pattern effects.

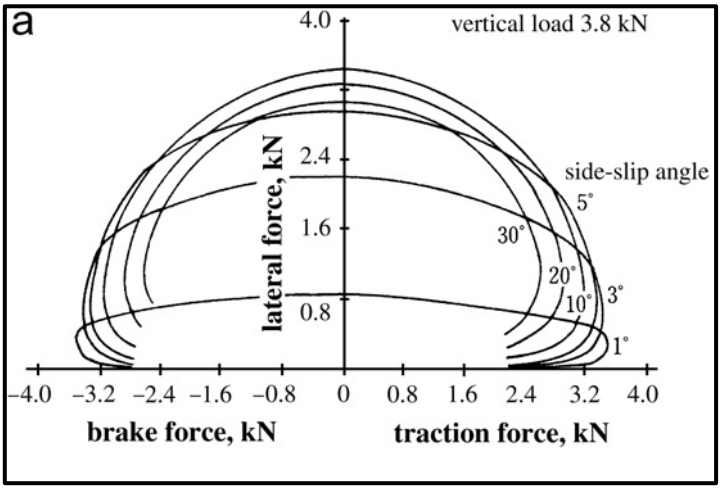

Figure 1.5 – The friction circle (a) and the effect of combined braking and turning (b). (Abe 2009: 36)

1.2.2.3 Cornering

In order for a vehicle to change direction, it follows from Newton's First Law (which states that an object will remain at rest or will move with a uniform velocity if there is no resultant force acting on it (Meriam and Kraige 2003: 6)) that a force in the lateral direction is required. As indicated in Figure 1.4, the lateral force increases as the side-slip angle increases (Gillespie 1992: 198).

Newton's Second Law (the acceleration of an object is proportional to the sum of forces acting on it (Meriam and Kraige 2003: 6)) is used to derive the steady-state cornering equations (steady-state indicating that cornering is occurring at a constant longitudinal speed along a curve with constant radius). Gillespie (1992: 199) states that the sum of forces in the lateral direction is the summation of the lateral forces developed at the front and rear wheels and these forces must equal the centripetal acceleration, or:

$$\sum F_y = F_{yf} + F_{yr} = \frac{MV^2}{R} \qquad (1.3)$$

When cornering at low speeds, the minimum negotiable radius is the turning radius of the vehicle, which is determined by the vehicle's geometry. However, when cornering at high speeds, the limit to path curvature is not the amount the wheels can turn but rather the maximum centripetal force that can be generated at the contact patches (this is deduced from Equation (1.3)). Blundell and Harty (2004: 401) state that the maximum lateral force which may be developed by the tyres is governed by the friction coefficient between the tyres and the road. Equation (1.4) shows that the maximum lateral acceleration achievable is equal to the friction coefficient (in units of *g*):

$$\frac{A_y}{g} = \frac{F_y}{Mg} = \frac{Mg\mu}{Mg} = \mu \tag{1.4}$$

1.2.3 Trajectory planning

Due to the limits imposed on the forces acting on the vehicle by the tyre-road interface, it follows that there will be a limit to the accelerations the vehicle can experience during driving. These limits can be reached during driving in a straight line when the wheels lock due to hard braking or spin during hard acceleration. When cornering at a constant speed, reaching the lateral force (and thus acceleration) limits will cause the vehicle to slide or spin out. Combined manoeuvres such as braking in a turn can result in both lateral and longitudinal limits being reduced due to the effects of the friction circle.

The question thus to be addressed is what is the optimum trajectory that should be followed by a vehicle when performing a manoeuvre. By optimizing the trajectory the probability of losing control of the vehicle is lowered. The word trajectory is used, since the path to be followed lies between two bounds (i.e. the left and right boundaries of the road or track being driven).

Braghin *et al.* (2011) developed an approach to identify the optimal trajectory for a race driver. Two trajectory planning approaches are proposed by Braghin *et al.* (2011), depending on the application. The first approach is the minimum space trajectory (resulting in the shortest distance) and the second the minimum curvature trajectory (resulting in maximum speed and thus minimum time) (Braghin *et al.* 2011); minimizing the curvature of the trajectory (which implies a larger turning radius) results in minimizing the lateral acceleration experienced by the vehicle (see Equation 1.3). Reducing the lateral acceleration reduces the lateral force applied to the tyres, allowing higher longitudinal forces to be developed in the tyre contact patch without exceeding the tyre's limits (staying within the friction circle) (Gillespie 1992: 199), or increasing the speed at which the trajectory can be followed.

The approaches followed by Braghin *et al.* (2011) rely on discretizing the road the vehicle has to follow into segments. Given the road's centreline coordinates, the left and right edges (or boundaries) of the road are then determined by assuming a track width (or using the actual measured track width). The position of the vehicle on the road (which must lie within the bounds of the road) is then given by Equation (1.5), where the position depends on the variable α (which is allowed to vary between zero and unity, zero resulting in the position being on the right boundary and unity on the left boundary) (Braghin *et al* 2011):

$$P = x_r + \alpha(x_l - x_r)\hat{\boldsymbol{\imath}} + y_r + \alpha(y_l - y_r)\hat{\boldsymbol{\jmath}} \tag{1.5}$$

Braghin *et al* (2011) then formulates a bound quadratic optimisation problem which, depending on the formulation, results in the shortest distance of minimum curvature trajectory, with α being the independent variable to be optimized. The cost function of the quadratic optimisation problem for the shortest distance trajectory is formulated from the distance formula in Cartesian coordinates:

$$S^2 = \sum_{i=1}^{n_{seg}} \Delta P_i^2 \tag{1.6}$$

where

$$\Delta P_i = \Delta P_{x,i}\hat{\boldsymbol{\imath}} + \Delta P_{y,i}\hat{\boldsymbol{\jmath}} \tag{1.7}$$

After some mathematical manipulation and substitution, Equation (1.6) may be written as (Braghin *et al* 2011):

$$S^2 = \frac{1}{2}\langle\alpha_s\rangle[H_s]\{\alpha_s\} + \langle B_s\rangle\{\alpha_s\} + const \tag{1.8}$$

A similar approach is followed to formulate the cost function for the minimum curvature trajectory. The curvature of a line in the Cartesian coordinate-system is given by (Stewart 2003: 864):

$$\kappa^2 = \left(\frac{d^2x}{ds^2}\right)^2 + \left(\frac{d^2y}{ds^2}\right)^2 \tag{1.9}$$

Further mathematical manipulation and substitution provide the cost function of the minimum curvature trajectory formulation given by Equation (1.10):

$$\kappa^2 = \frac{1}{2}\langle\alpha_\kappa\rangle[H_\kappa]\{\alpha_\kappa\} + \langle B_\kappa\rangle\{\alpha_\kappa\} + const \tag{1.10}$$

As mentioned earlier, the independent variable α is allowed to vary between zero and unity. The quadratic programming problems formulated by Braghin *et al* (2011) are thus cases of bound optimisation problems, with no other imposed constraints. Examples of the results of optimising the trajectory for both shortest distance and minimum curvature are shown in Figure 1.6 (Braghin *et al* 2011).

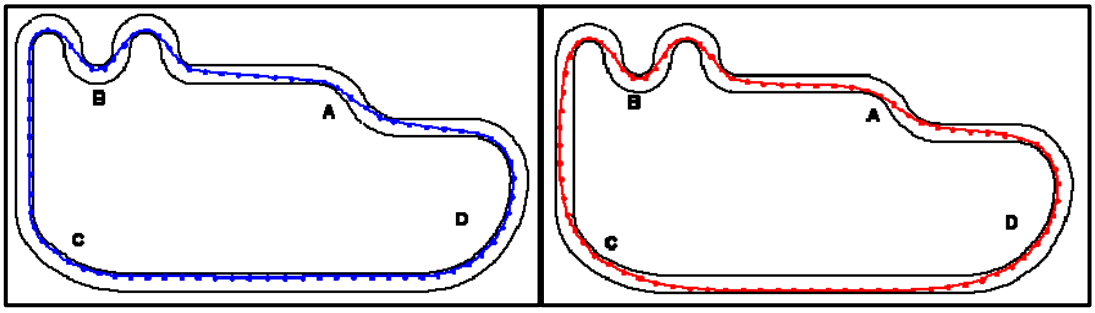

Figure 1.6 – Optimised trajectory for shortest distance (left) and minimum curvature (right) (Braghin *et al* 2011)

1.2.4 Driver models

Research into the dynamics that describe an automobile's behaviour has been conducted since the early 1940s and through the formulation of differential equations a basic understanding of the vehicle system dynamics has been attained. However, it was not until the 1960s that the driver of the automobile and the effects of this human-machine system were considered. With the introduction of driver assistance systems and the emphasis on the modelling and simulation of vehicle behaviour, the need for capable driver models have become obvious (Plöchl and Edelmann 2007).

1.2.4.1 Human based driver models

Driver models are required for closed-loop handling simulations. More specifically, when simulating a vehicle being driven by a human, the capabilities and limitations of a human driver need to be included. The attributes of a human driver include general driver skills and characteristics such as the ability to receive, perceive and process visual, vestibular, tactile and auditory information and to generate corresponding neuromuscular responses upon the processing of this information. Associated with this processing of information are time delays and limitations to processing abilities, but the ability to predict or anticipate the vehicle's dynamic behaviour is also essential to the human driver's skills (Plöchl and Edelmann 2007). MacAdam (2003) identified the key characteristics of the human driver that should be incorporated into any serious effort at modelling a human driver as:

- provision for a transport time delay
- making use of the driver's ability to 'look ahead', i.e. to sense upcoming lateral and longitudinal control requirements
- driver adaptation provision, i.e. to account for alterations to the controlled vehicle dynamics and operating conditions
- exhibition of a linear regime 'crossover model' in the immediate vicinity of the crossover frequency and
- the presence of an internal vehicle model – or an equivalent capability – within the structure of the driver model to help estimate future controlled vehicle responses.

A secondary set of desirable features of a human driver model that is not essential but, depending on the application should be included was also identified (MacAdam 2003):

- accounting for neural delays
- neuromuscular filtering elements for output channels such as steering, braking and throttle control responses
- previewed path adjustment by the driver model to account for driver skill-related abilities or preferences
- driver abilities to adjust speed based on upcoming lateral path requirements in order to facilitate safe negotiation of the prescribed path and avoiding obstacles
- provision for surprise or situational awareness features and

- inclusion of some form of driver skill factors.

1.2.4.2 Vehicle based driver models

The use of human based driver models is advantageous during the development of vehicles to be driven by humans. In the case of the autonomous control of a vehicle, the driver model used need not include the human characteristics as discussed above. The performance of autonomous vehicles is not limited to human behaviour and capabilities. Botha (2011) identified three types of vehicle derived controllers, namely geometric, kinematic and dynamic controllers. The geometric and kinematic controllers are the simplest, since a no slip assumption is made.

A geometric driver model makes use of the geometric relationships between the wheel base, steering angle and radius of curvature of the road. Geometric models often make use of the Ackerman or bicycle models and the preview distance and cross-track error are then obtained through a combination of the turning radius and the steering angle (Botha 2011). The problem with using these models for control purposes is that the Ackerman and bicycle models were developed for low speed cornering – the tyres need not develop lateral forces and lateral movement is due to the geometry of the system (Gillespie 1992: 196).

A kinematic controller is a based on a model of the motion of the individual parts of the system without reference to the forces causing this motion (Meriam and Kraige 2003: 3). Botha (2011) states that the most basic kinematic controllers make use of the bicycle model to derive the equations for longitudinal and lateral motions and use the steering angle, wheel base and vehicle speed to determine vehicle heading. The kinematic driver models were found to provide improved control compared to the geometric driver models, but at high cornering speeds (where the slip in the contact patch becomes significant) the vehicle becomes unstable (Botha 2011).

The dynamic driver model is the only model which takes into account the forces developed in the contact patch and hence introduces the mechanism of slip. In 2011 Botha developed two dynamic driver models. The first dynamic driver model made use of MSC.ADAMS/View simulations to construct the relationship between the steady state yaw acceleration vs. steer rate as a function of vehicle speed. The second dynamic driver model uses a linear vehicle model as a basis. The model is used to obtain a transfer function which may then be used for control purposes. Included in this model are the effects of load transfer and the non-linear tyre effect by the use of a sliding mode. These driver models developed by Botha (2011) were experimentally validated and exhibited good stability at high speeds. However, these driver models only provided for the lateral requirements of path following (more on this in Section 2.3.1).

1.3 Conclusion

The literature survey has shown that several projects have been completed successfully in the field of developing autonomous vehicles. These autonomous vehicles (such as Stanley) mainly operate at low speed. When considering Figure 1.4, one may conclude that at low speed (and

thus low slip angle) the behaviour of the vehicle is almost linear. The challenge in controlling a vehicle at low speed is mainly in the decision making process, optimising the software architecture and then sending the correct signals to the actuators. These control systems largely neglect, simplify or linearize the vehicle dynamics, and operate well within the vehicle's capabilities.

Several projects at the University of Pretoria are aimed at developing an autonomous ground vehicle that operates at high speed, specifically addressing high speed cornering. These projects have taken the full vehicle suspension and tyre non-linearity into account. Control systems that mimic a driver's inputs have also been developed and while these control systems function as intended, they have not been integrated into a single control system which provides guidance and navigation fully autonomously to the Land Rover test vehicle. Furthermore, a control algorithm that controls the velocity of the experimental vehicle has not been developed.

1.4 Project plan

The research question of this project may thus be defined as: to develop an autonomous longitudinal control system for path planning and following that takes into account the non-linear vehicle dynamics and uses GPS information for path preview. This control system should prevent the vehicle from exceeding the limits imposed by the vehicle dynamics and hence improve the safety of the occupants. The control system is based on trajectory planning algorithm developed by Braghin *et al.* (2011). Braghin *et al*. (2011) developed a similar control system and evaluated its performance with a simplified dynamic model. The results reported by Braghin *et al.* (2011) indicated that developing a control system based on optimizing the path of a vehicle may result in improved lap times for race drivers. The same approach is followed in this paper but now with the focus on reducing lateral acceleration of the vehicle and hence improving vehicle safety rather than decreasing lap time around a racetrack.

A model-based design approach will be followed to develop the longitudinal control system and an experimentally validated model is thus required. An existing MSC.ADAMS/View multi-body dynamics model that accurately captures the fully nonlinear vertical and lateral dynamics of the test vehicle has been developed by Uys *et al.* (2007). The model is now expanded and experimentally validated to accurately capture the longitudinal dynamics.

The driver models developed by Botha (2011) have been updated and improved to provide for a trajectory planning algorithm, based on the work done by Braghin *et al.* (2011). The longitudinal control system is developed in simulation and finally validated experimentally.

Successful completion of the project thus depends on the following:

1. Development of a longitudinal model for the model of the experimental vehicle in MSC.ADAMS/View. This model must be characterised and validated experimentally.
2. The driver models developed by Botha (2011) have to be updated and improved to provide for a trajectory planning algorithm, based on the work done by Braghin *et al.* (2011).

3. The MSC.ADAMS/View model will then be used to develop a control system that prevents the vehicle from exceeding predefined lateral acceleration limits by limiting vehicle speed. This control system will be developed as a driver assist system, rather than a fully autonomous control system.
4. The developed speed control system has to be implemented on the experimental vehicle.
5. The results from the experimental implementation of the control system have to be compared to the simulation results found in Step 3.

Chapter 2

Development and validation of longitudinal vehicle simulation model

We were hoping to have a working model on display; instead we have simulations

– Rob Davis (1964-) Canadian politician

2.1 Introduction

The benefits of simulation in the modern engineering fraternity are numerous. Simulation models lead to a better understanding of the design variables, rapid experimentation without building a prototype and optimisation of the design without costly iterations.

However, simulation models are often not reliable unless experimentally validated. The goal of model validation is to make the model useful in the sense that it accurately represents the system being modelled so that accurate information with regards to the behaviour of the system being modelled is produced. Experimentally validating a model of a physical system thus lends credibility to the behaviour predicted by the model when simulating a certain set of inputs, which may not have been experimentally tested on the physical system.

This chapter discusses existing autonomous actuators and control systems already fitted to the land Rover test vehicle, as well as the development and validation of a mathematical model of the Land Rover Defender test vehicle to be used to simulate the dynamic behaviour of the Land Rover in response to the inputs given by the artificial intelligence used to control the vehicle.

2.2 Vehicle instrumentation

For the purpose of experimental validation of the vehicle simulation models developed by the Vehicle Dynamics Group (VDG) at the University of Pretoria, an array of measurement equipment has been installed on the Land Rover test vehicle. A PC/104 form factor embedded computer is used in conjunction with a Diamond-MM-AT 12-bit Analogue I/O Module (Diamond Systems

Corporation 2004). This I/O module has sixteen analogue inputs with 12 bit resolution, two analogue outputs,

Table 2.1 – Measured variables

Variable measured	Sensor	Signal
Engine speed	Proximity switch with frequency to voltage converter	Analogue
Driveshaft speed	Proximity switch with frequency to voltage converter	Analogue
Driveshaft torque	Strain gauges	Analogue
Wheel speed left front	Proximity switch with frequency to voltage converter	Analogue
Wheel speed right front	Proximity switch with frequency to voltage converter	Analogue
Yaw velocity	Solid state gyroscope	Analogue
Roll velocity	Solid state gyroscope	Analogue
Pitch velocity	Solid state gyroscope	Analogue
Brake line hydraulic pressure	Pressure transducer	Analogue
Brake actuator pneumatic pressure	Pressure transducer	Analogue
Right front kingpin angle	Rotary potentiometer	Analogue
Steering wheel angle	Rotary potentiometer	Analogue
Throttle angle	Rotary potentiometer	Analogue
Vehicle speed	GPS	Analogue
Gear lever extended	Proximity switch	Digital
Gear lever retracted	Proximity switch	Digital
Gear rail extended	Proximity switch	Digital
Gear rail retracted	Proximity switch	Digital
Clutch extended	Proximity switch	Digital
Clutch retracted	Proximity switch	Digital

eight digital inputs and eight digital outputs. The variables measured during vehicle tests are summarised in Table 2.1.

2.3 Actuators and control systems fitted to the test vehicle

There are several actuators with feedback control systems implemented on the Land Rover Defender test vehicle. This section aims to give a brief overview of the systems in the Land Rover and the controlling actuators developed by the Vehicle Dynamics Group.

2.3.1 Steering control system

The steering system on the Land Rover Defender consists of a drag link and track rod which is complemented by a power steering system that is belt driven from the engine (Rover Group Limited 1996). The University of Pretoria's Land Rover has been fitted with a steering robot,

which comprises of a FESTO stepper motor that is connected to the steering box of the vehicle via two universal joints and a toothed belt drive (see Figure 2.1 (Botha 2011)).

Botha (2011) developed two robust driver models capable of path following at both high and low vehicle speeds. These models were implemented and validated experimentally on the Land Rover where the vehicle successfully negotiated a severe double lane change manoeuvre (ISO 3888-1:1999) at 80km/h – very close to the vehicle's limits.

Figure 2.1 – Photo of steering robot installed on the Land Rover (Botha, 2011)

2.3.1.1 Magic Formula yaw angle controller

The steering controller developed by Botha and Els (2011) is based on the observation that for a given constant steering input rate the vehicle obtains constant steady state yaw acceleration. While this phenomenon is true for all vehicle speeds, the response tends to diminish near the region of lateral tyre force saturation as shown in Figure 2.2. Full tyre saturation occurs at approximately 8.5m/s^2 lateral acceleration.

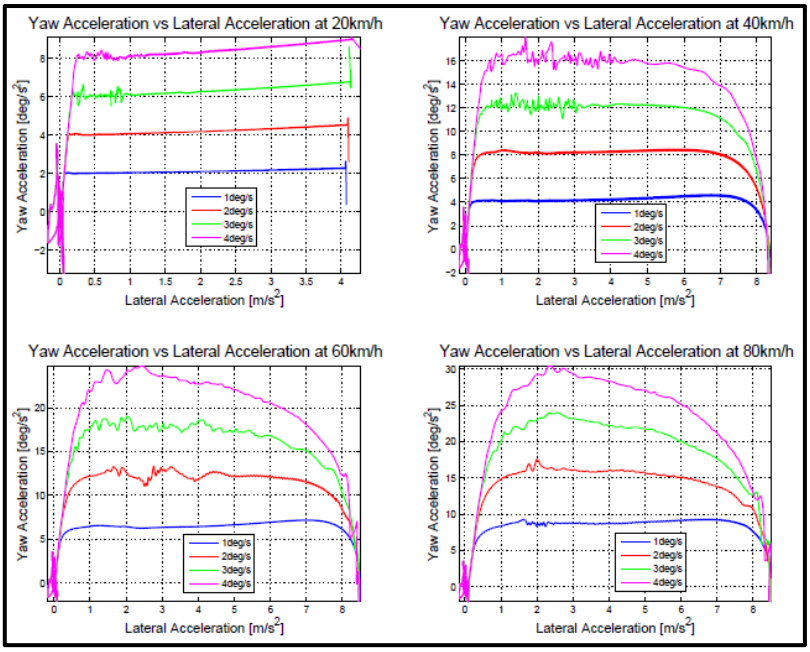

Figure 2.2 – Yaw acceleration response as a function of steer rate, vehicle speed and lateral acceleration (Botha and Els, 2011)

From Figure 2.2 a steady state yaw acceleration can be obtained and plotted as a function of steer rate for each vehicle speed. This is shown in Figure 2.3. It may further be seen in Figure 2.2 that the trend between yaw acceleration and steer rate relationship resembles that of the lateral tyre force vs. side-slip for different wheel loads. A Magic Formula (Bakker *et al.,* 1989) curve fit was used to approximate the relationship between the yaw acceleration and the vehicle speed and steer rate, as shown in Figure 2.3 (Botha and Els, 2011).

$$\ddot{\psi} = 2\frac{\psi_d - \psi_0 - \dot{\psi}\tau}{\tau^2} \tag{2.1}$$

The desired yaw acceleration needed to obtain a specific yaw angle was determined using Equation (2.1). Having modelled the relationship between yaw acceleration and steer rate with the Magic Formula (Bakker *et al.*, 1989) curve fit, the required steer rate was written as the subject of the control equation. This equation has three possible solutions each representing different parts of the relationship containing multiple terms. Rather than trying to solve this equation analytically, Botha and Els (2011) used a Feed Forward Neural Network (FFNN) find the solution. Using a FFNN greatly simplified the implementation and improved computational efficiency. Equation (2.2) was used to determine the required steering rate input.

$$\dot{\delta}_{\psi,FFNN} = \dot{F}FNN(\psi,\ddot{V}) \tag{2.2}$$

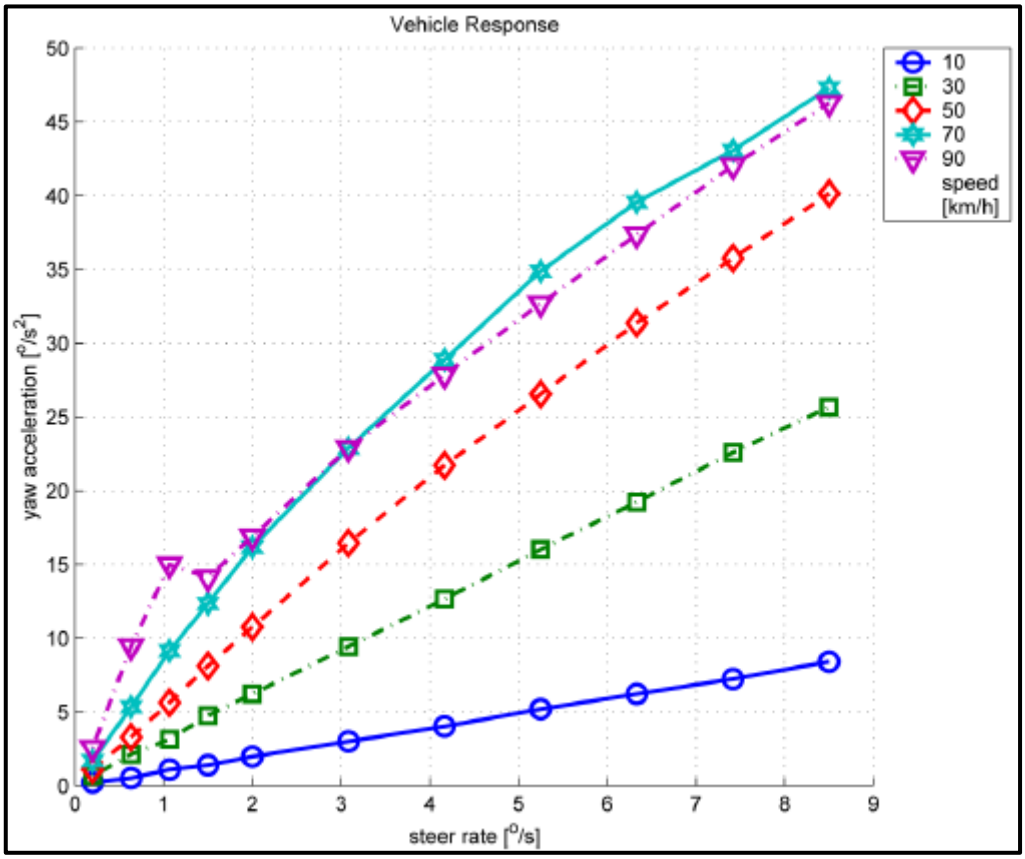

Figure 2.3 – Yaw acceleration as a function of lateral acceleration for various vehicle speeds and steering rates (Botha and Els, 2011)

2.3.1.2 Lateral position control

While the yaw angle controller described in Section 2.3.1.1 strives to keep the vehicle parallel to the prescribed path, the accumulation of errors may lead to a lateral offset from the prescribed path. As a result the yaw angle controller was complemented by Botha and Els (2011) with a controller that minimises the lateral error at a set distance ahead of the vehicle. A gain scheduling Proportional Derivative (PD) controller, used to minimise the lateral error, was implemented. The gain scheduling is introduced to compensate for the increase in steering sensitivity as vehicle speed increases. This controller gives minimal control action and is mainly used to reduce the accumulation of lateral errors.

2.3.2 Braking control system

The standard braking system implemented on the Land Rover consists of disc brakes on all four wheels. The front brakes operate on separate hydraulic lines and the rear brakes on a shared hydraulic line. The brakes are actuated from the pedal assembly, which consists of a brake pedal, booster and master cylinder. A schematic representation is shown in Figure 2.4 (Rover Group Limited 1996).

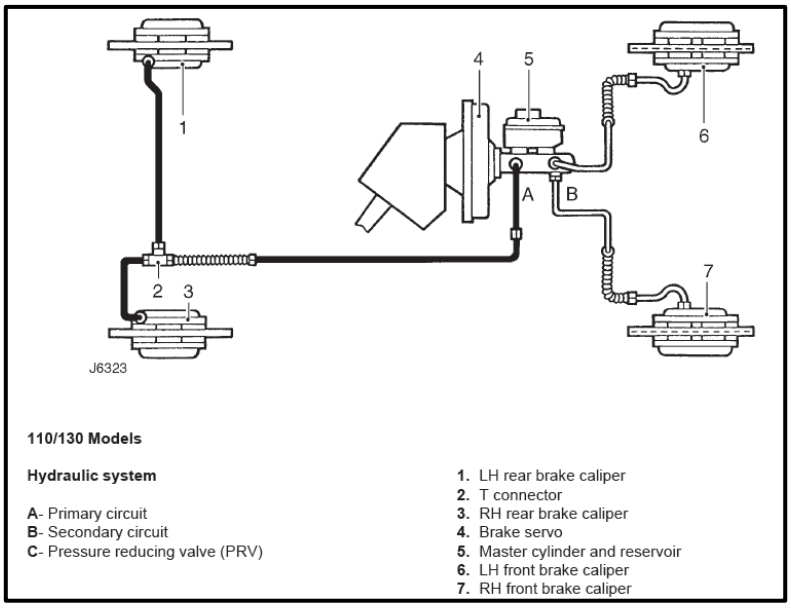

Figure 2.4 – Schematic layout of Land Rover hydraulic brake system (Rover Group Limited, 1996)

In 2008, an actuator and control system was implemented to enable autonomous control of the braking system (Botha, 2008). A pneumatic cylinder was connected to the brake pedal via a pneumatic piston rod and a connector (this design is similar to the design of the clutch control actuator discussed in Section 2.3.3 and Figure 2.6). The 2008 design relied on normal two-way valves to regulate the pressure in the cylinder and hence the pneumatic cylinder was only used in retraction (i.e. depressing the brake pedal), relying on external springs to bring the piston back to its original position (Botha, 2008). The system relied on feedback from a pneumatic pressure

transducer and a PID controller to control the pressure in the pneumatic cylinder and hence the brake actuation (and vehicle deceleration).

Botha (2008) concluded in his report that this system performed to specification, but that some issues were experienced when the pedal had to return to its initial (or off) position due to the fact that external springs were used. He recommended the implementation of proportional valves to enable control of the pneumatic cylinder in both directions as well as using feedback from the hydraulic braking system rather than the pneumatic cylinder pressure.

Mathebula (2009) subsequently improved the braking system by implementing some of Botha's recommendations. He implemented proportional valves and relocated the feedback from the pneumatic cylinder to the hydraulic brake line pressure. These modifications allowed the implementation of control systems that act as driver assists such as traction control and hill assist.

A major problem experienced by both Botha (2008) and Mathebula (2009) were the limitations imposed on the autonomous control system due to the use of pneumatic actuators. It was found by Botha that the reservoir pressure dropped to below 7bar (the operating pressure) after performing two hard braking tests. It was thus recommended by Botha (2008) that the problem of supplying air, at a pressure of at least 7bar continuously, be addressed.

2.3.3 Gear-shift and clutch control system

The Land Rover test vehicle is equipped with an all synchromesh five speed manual gearbox. The gear change has a single rail selector and spool type interlock. The clutch unit comprises a single dry plate friction disc and diaphragm spring clutch, which is secured directly to the engine flywheel. The clutch unit is operated hydraulically by the clutch master cylinder and slave cylinder attached to the transmission bell housing (Rover Group Limited 1996). The clutch pedal and plate assembly is shown in Figure 2.5.

Barnard (2008a) developed a control system that disengages the Land Rover's clutch, selects a gear and then engages the clutch. The system allows control of the vehicle's clutch and gear shift from a computer (or manually) and is actuated pneumatically.

A FESTO pneumatic actuator was used in retraction to actuate the clutch pedal and hence control the position of the clutch. The operating pressure is 6bar as recommended by the FESTO pneumatic drive catalogue (Barnard 2008a). The clutch return spring is used to return the clutch pedal to its engaged position. Flow rate regulators are used to control the rate of actuation. A fuzzy logic controller was implemented to control the clutch pedal actuator and allows the vehicle to perform smooth clutch engagements by monitoring engine and driveshaft speed (Barnard 2008b).

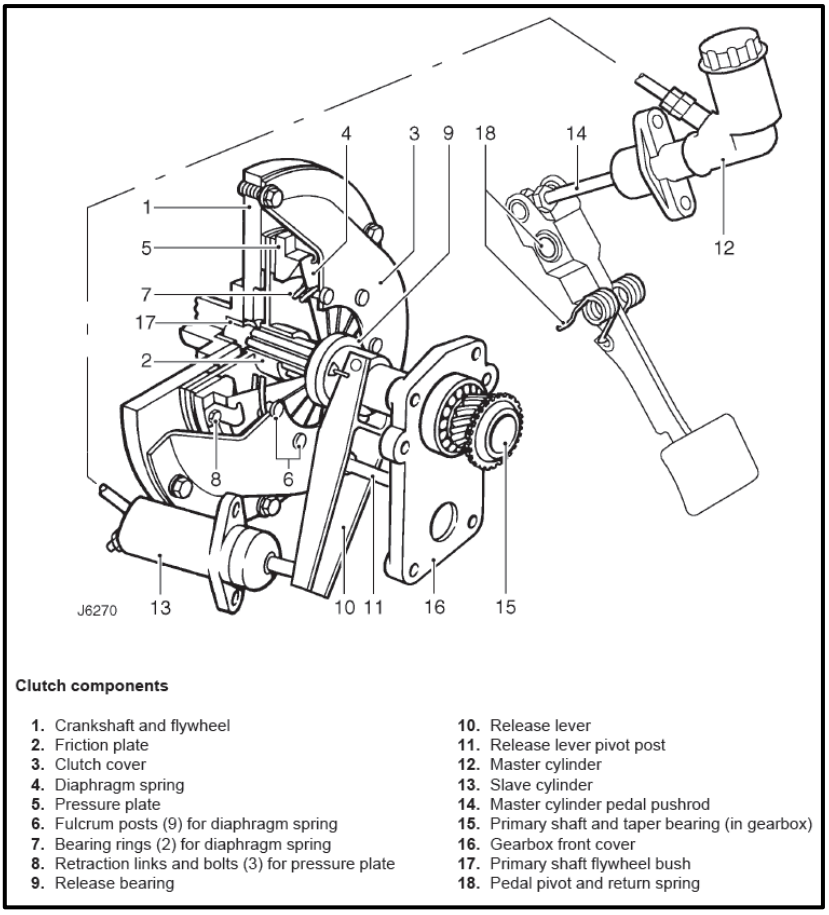

Clutch components

1. Crankshaft and flywheel
2. Friction plate
3. Clutch cover
4. Diaphragm spring
5. Pressure plate
6. Fulcrum posts (9) for diaphragm spring
7. Bearing rings (2) for diaphragm spring
8. Retraction links and bolts (3) for pressure plate
9. Release bearing
10. Release lever
11. Release lever pivot post
12. Master cylinder
13. Slave cylinder
14. Master cylinder pedal pushrod
15. Primary shaft and taper bearing (in gearbox)
16. Gearbox front cover
17. Primary shaft flywheel bush
18. Pedal pivot and return spring

Figure 2.5 – Clutch pedal and plate assembly (Rover Group Limited, 1996)

The gear control unit comprises two pneumatic FESTO actuators that control the translation (forwards-backwards) and rotational movements (left-right) of the gear lever. A computer controller is responsible for actuating the gear lever according to predetermined shifting protocols. Once again flow rate regulators are used to control the rate of actuation at a pneumatic operating pressure of 6bar (Barnard 2008a). The gear control unit is capable of both sequential and non-sequential shifting and maintains the gear lever in the desired position when the pressurised air supply is removed (Barnard 2008b). A CAD assembly of the clutch actuator is shown in Figure 2.6.

Barnard (2008b) recommended that the system be improved by reducing the number of cables used for data transfer and addressing the pressurised air supply problems also experienced by Botha (2008) and Mathebula (2009) with the automated braking system.

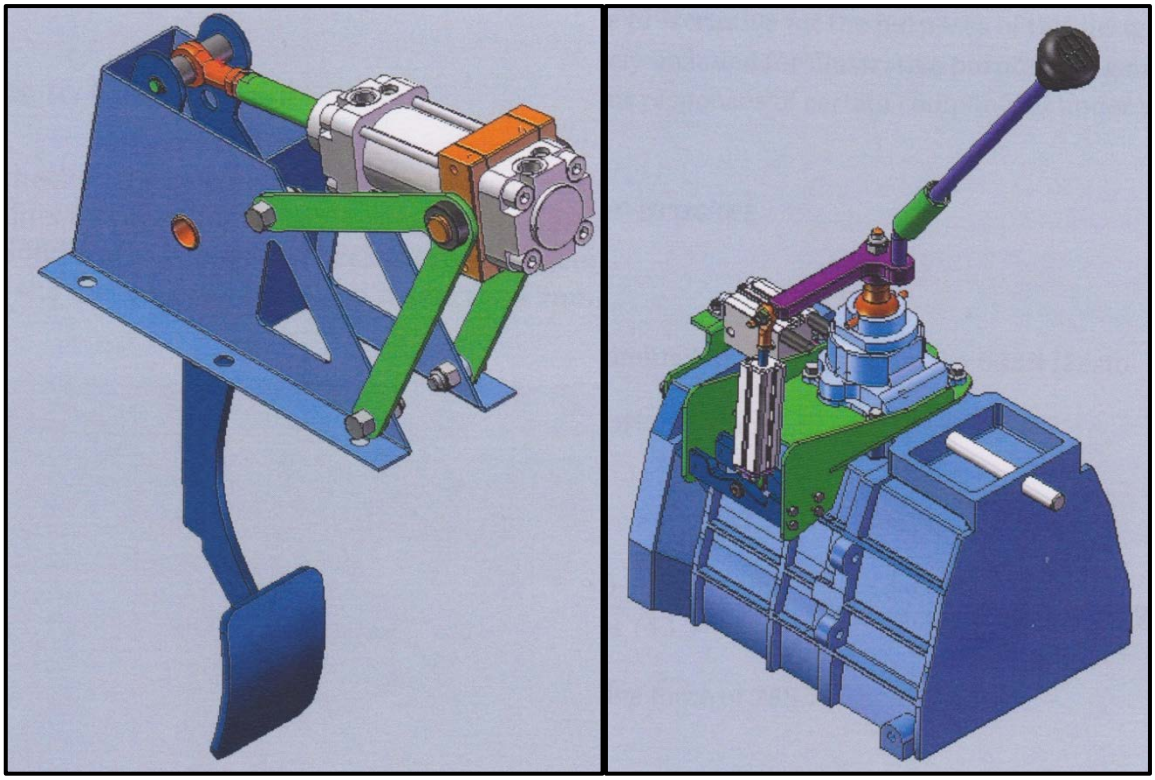

Figure 2.6 – CAD assembly of clutch pedal actuator (left) and gear shift actuators (right) (Barnard 2008a)

2.3.4 Throttle control system

A stepper motor was implemented to control the throttle pedal position in 2011. The stepper motor pulls a cable which runs over a number of pulleys, which then increases the throttle position. External springs are used to return the throttle pedal to its zero position (Hamersma 2011). A proportional gain feedback control system that uses a single-turn potentiometer for feedback purposes was used to maintain a desired throttle position.

It was recommended by Hamersma (2011) that the throttle pedal actuator be improved and the return of the throttle pedal to the zero position be directly controlled with the stepper motor, rather than relying on external springs. Not only will this improve the control of the throttle pedal position, but it may also improve the ergonomics of the driving position when not operating the vehicle in autonomous mode.

The throttle pedal system was upgraded to incorporate an HTD toothed belt and pulley system, rather than the cable system. The advantage of implementing the belt and pulley system is that the throttle position can now be controlled in both increasing and decreasing directions without relying on cumbersome external springs. The improvement also leaves more space in the foot well, resulting in a more ergonomic driving position when not operating the vehicle autonomously. The 3D assembly of the actuator is shown in Figure 2.7.

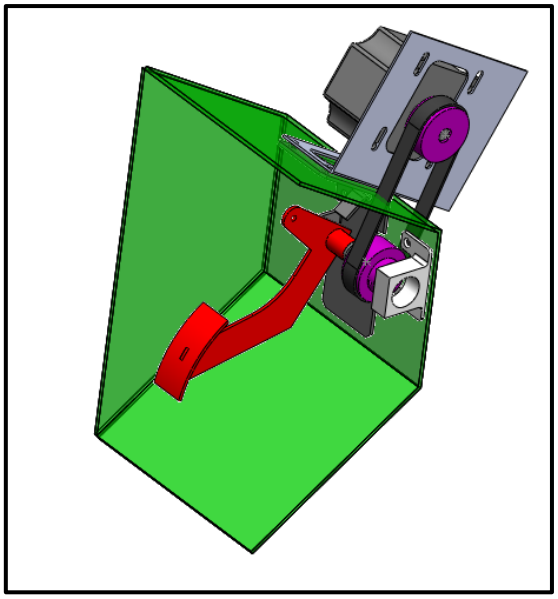

Figure 2.7 – CAD assembly of throttle pedal actuator

2.4 The ADAMS model

An integral part of the vehicle engineering research at the University of Pretoria is the development of a validated model of the Land Rover test vehicle. The model, which was developed jointly in MSC.ADAMS/View and MATLAB's Simulink package, is used to simulate manoeuvres and tests that would typically be performed on a prototype vehicle. The most significant advantages of using simulation models are given by Blundell and Harty (2004: 400) as:

- better understanding of the design variables
- rapid experimentation without building a physical prototype, reducing costs considerably and
- optimisation of the design.

A 16-degree of freedom, fully non-linear vehicle dynamics model of the Land Rover test vehicle was developed by Thoresson (2007) and then modified and updated by Uys *et al* (2007) and Cronje (2008). The model successfully captures the non-linear spring and damper characteristics, non-linear bump stops and bushes as well as body torsion about the longitudinal axis. The model implements the Pacejka '89 tyre model. The MSC.ADAMS/View model was further updated to include driveline dynamics by Hamersma (2011). Botha (2011) also included the path following capabilities required for his research. Further expansion of the model is thus needed to include the brakes, engine braking, and demand forces. Hamersma (2011) recommended further refinement of the engine map.

The model is expanded to allow for inputs as generated by the autonomous control system, i.e. the state variables controlled by the various actuators will be given as input to the model. The inputs to the model (for longitudinal control purposes) are:

- throttle pedal position
- brake line hydraulic pressure
- clutch position and
- gear selection position.

A graphical representation of the ADAMS model is shown in Figure 2.8 and the basic vehicle parameters are provided in Table2.2.

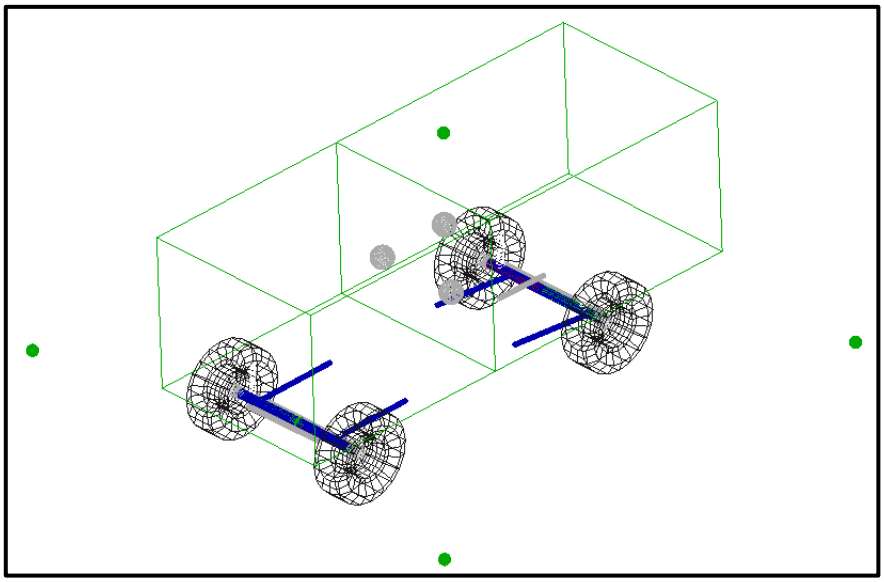

Figure 2.8 – Graphical representation of ADAMS model

Table 2.2 – Basic vehicle parameters

Parameter	Value	Unit
Total vehicle mass	2047	kg
Vehicle sprung mass	1576	kg
Mass moment of inertia	2057	kgm^2
Distance from front axle to CG	1.4	m
Distance from rear axle to CG	1.4	m
Track width (front and rear)	1.486	m
Distance between left and right $4S_4$ struts	1.009	m
Front roll centre height	0.3985	m
Rear roll centre height	0.517	m
Roll centre to CG	0.14	m
Tyre cornering stiffness	36821	N/rad
Drag coefficient	0.63	dimensionless
Coefficient of rolling resistance	0.024	dimensionless
Rolling radius	0.386	m

2.5 Modelling the longitudinal dynamics

The supply and demand forces (as described by Equation (1.1)) as developed by the Land Rover test vehicle had to be characterised experimentally. These characteristics were then included in the existing MSC.ADAMS/View model of the Land Rover.

2.5.1 The supply forces

The standard procedure to characterise a vehicle's engine is to use the wide open throttle (WOT) torque map, however, these WOT torque maps are usually determined under laboratory conditions with no parasitic loads (such as power steering and air conditioning) applied to the engine. Furthermore it has to be noted that the Land Rover Defender has more than 120 000km on the odometer and will be tested at altitudes of 1700m above sea level. With regards to the gearbox , transfer case and differential ratios, it must be noted that during the production run of the Land Rover Defender in the 1990s the gearboxes, transfer cases and differentials fitted to the Land Rover Defender was continuously updated and altered. It was thus deemed safer to experimentally determine the engine and power train characteristics rather than relying on possibly erroneous published technical specifications.

The torque delivered by the engine is a function of two parameters, namely engine speed and throttle position. To determine the torque delivered by the engine, strain gauges were applied to both forward and rearward drive shafts of the Land Rover Defender in a full-bridge configuration. The strain gauges were calibrated in the laboratory for direct torque measurement by applying known torque values. Figure 2.9 shows the calibration setup. Binsfeld Engineering's TorqueTrak 9000 Digital Telemetry System (Binsfeld Enineering Inc.) was used to measure the torque applied at a constant throttle position as maintained by the throttle pedal actuator.

Figure 2.9 – Driveshaft torque calibration setup

Characterisation of the gearbox, transfer case and differential ratios along with the wheel rolling radius was thus necessary to determine the engine torque, since it is being measured on the driveshaft. By measuring the engine speed and propeller shaft speed for various gear selections, the gear ratios and transfer case ratios were determined.

Similarly, by comparing the wheel speed and propeller shaft speed, the differential ratio was determined. The rolling radius was measured as the distance from the centre of the wheel to the road on a flat road under static wheel load. Table 2.3 summarizes these measurements (Note that the gear ratios include the transfer case ratio). These ratios were previously implemented in the MSC.ADAMS/View model of the Land Rover by Hamersma (2011).

Table 2.3 – Gear ratios, differential ratios and rolling radius

Variable	Ratio
First gear	5.158:1
Second gear	2.764:1
Third gear	1.737:1
Fourth gear	1.202:1
Fifth gear	0.888:1
Differential	3.45:1
Rolling radius [m]	0.386

Tests were conducted by accelerating from idle speed until a constant vehicle speed was reached on a smooth and level concrete road (the Gerotek Long Straight). The throttle position was varied from 25% of the range of motion, to 100% (full throttle). The measured torque was then divided by the applicable gear ratio to find the engine torque, assuming 100% efficiency, i.e. the resulting torque compensates for inefficiencies in the gearbox and transfer case. The driveshaft speed was measured with a proximity switch and a frequency to voltage converter and multiplied by the applicable gear ratio to find the engine speed (although direct measurement of the engine speed is possible). The tests were repeated for various throttle positions, starting from idle speed until a constant speed was reached in various gears. The resulting torque is shown as a function of engine speed and throttle position in Figure 2.10.

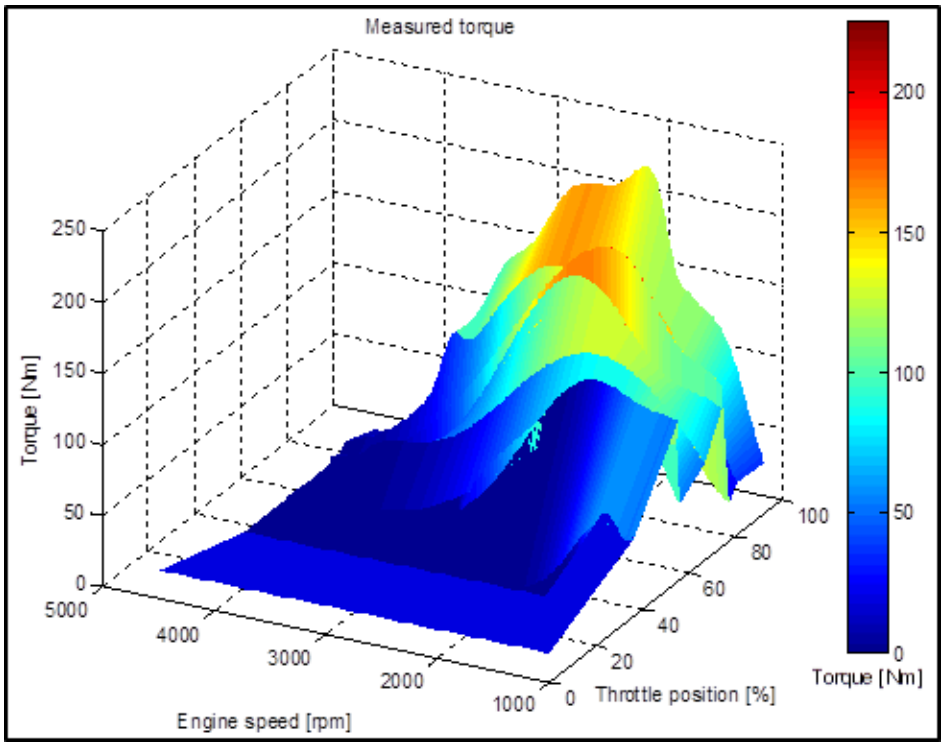

Figure 2.10 – Measured torque as a function of engine speed and throttle position

MATLAB's Surface Fit Toolbox was used to fit a polynomial function to the measured torque. To determine the goodness of the fit, the coefficient of determination was used (the coefficient of determination ranges between zero and unity, zero indicating no correlation and unity perfect correlation). The resulting fit had a coefficient of determination (R^2) of 0.93 and is shown in Figure 2.12. The resultant polynomial fit is given by Equation (2.3).

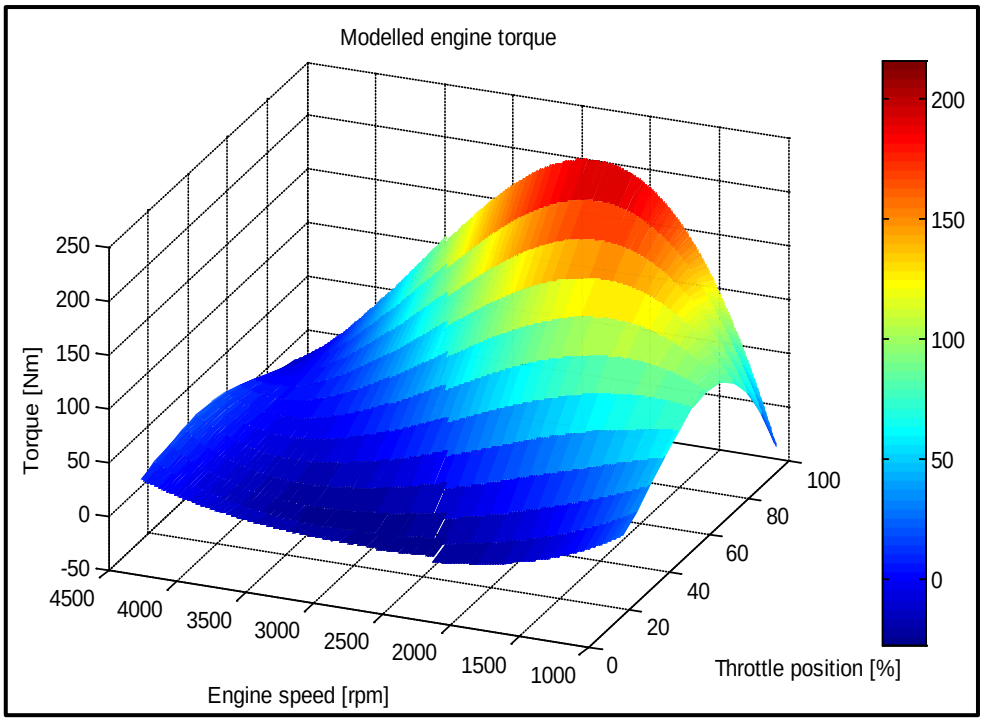

Figure 2.11 – Modelled torque as a function of engine speed and throttle position

$$T_{Engine} = p_{00} + p_{10}T + p_{01}n + p_{20}T^2 + p_{11}Tn + p_{02}T^2 + p_{30}T^3 + p_{21}T^2n + p_{12}Tn^2 + p_{03}T^3 + p_{40}T^4 + p_{31}T^3n + p_{22}T^2n^2 + p_{13}Tn^3 + p_{04}n^4 \quad (2.3)$$

with

$T = Throttle\ position$
$n = Engine\ speed$

$p_{00} = 62.52$
$p_{10} = 83.71$
$p_{01} = -64.18$
$p_{20} = 7.657$
$p_{11} = -32.87$
$p_{02} = -8.014$
$p_{30} = -3.583$
$p_{12} = 8.905$
$p_{21} = -30.6$
$p_{03} = 14.67$
$p_{40} = 1.834$
$p_{31} = 3.599$
$p_{22} = -11.74$
$p_{13} = 9.552$
$p_{04} = 1.366$

2.5.2 Drag and rolling resistance

Aerodynamic drag, rolling resistance and the gravity component due to inclination are the only demand forces acting on the vehicle. These forces are governed by Equation (1.1), which is repeated for continuity as Equation (2.4).

$$F_D = -F_{Brakes} - F_{Drag} - F_{rr} - F_{Incl} = -F_{Brakes} - {}^1/_2\,\rho V^2 C_D A_f - \mu_{rr} Mg\cos\theta - Mg\sin\theta \quad (2.4)$$

The demand forces due to drag and rolling resistance were determined by accelerating the vehicle to 100km/h and then coasting in neutral to a standstill on a level road while measuring the vehicle speed. Figure 2.12 plots the vehicle speed as a function of time. The vehicle speed is differentiated to find acceleration and also plotted in Figure 2.12 as a function of time. Applying Newton's Second Law the demand force is calculated from the acceleration. The demand force is shown as a function of vehicle speed in Figure 2.13.

As may be seen in Equation (2.4), the demand forces due to drag and rolling resistance (which in this case includes drivetrain drag and other losses) are a function of vehicle speed squared and a constant. A fit of this form was made through the captured data, resulting in the following coefficients:

$$\rho C_D A_f = (1)(0.63)(4.1) \quad (2.5)$$

$$\rho C_D A_f = 2.583$$

$$\mu_{rr} = 0.024 \quad (2.6)$$

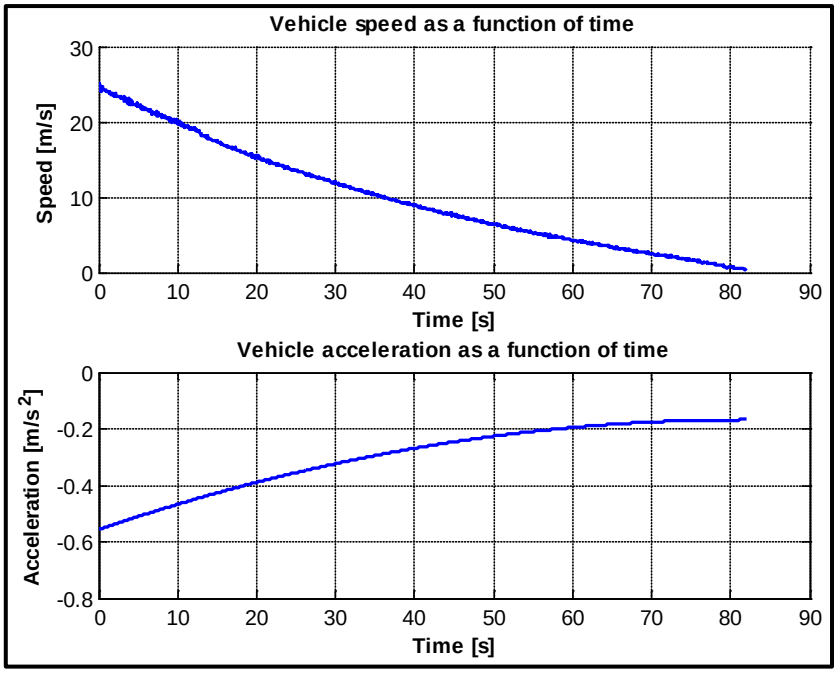

Figure 2.12 – Coast down experimental results

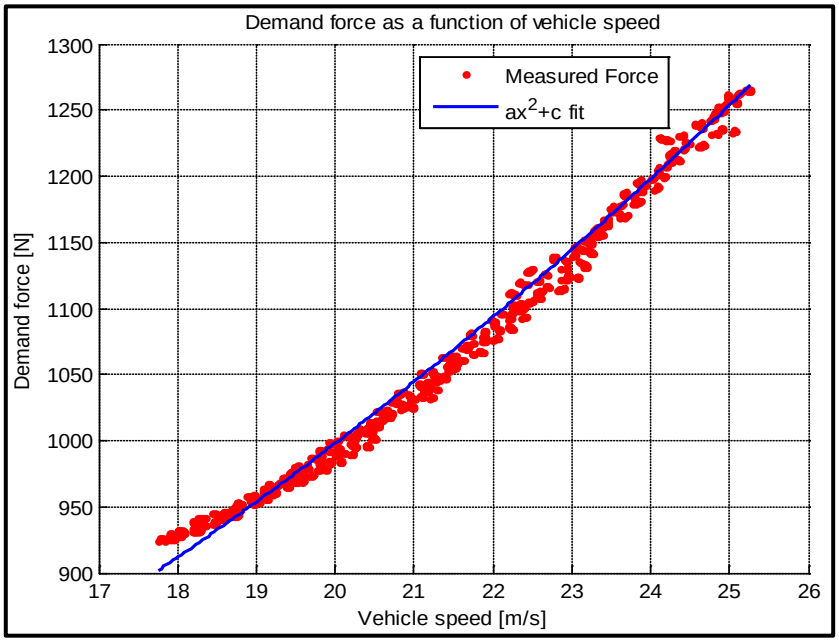

Figure 2.13 – Demand force due to drag and rolling resistance as a function of vehicle speed

2.5.3 Engine braking torque

The engine braking torque is applied to the power train when the driver removes his/her foot from the throttle pedal while the vehicle is moving and in gear. This is due to the torque required to turn the engine while compressing the air inside the cylinders. This torque is multiplied by all the gear, transfer case and differential ratios that form part of the vehicle's power train and is applied to the driving wheels. Characterisation of the engine braking torque was done by Botha

(2008), and the governing equation is given by Equation (2.7). Equation (2.7) is plotted in Figure 2.14.

$$T_{EBT} = 3.8713 \times 10^{-6} n^2 - 25.11 \times 10^{-3} n + 5.44 \quad (2.7)$$

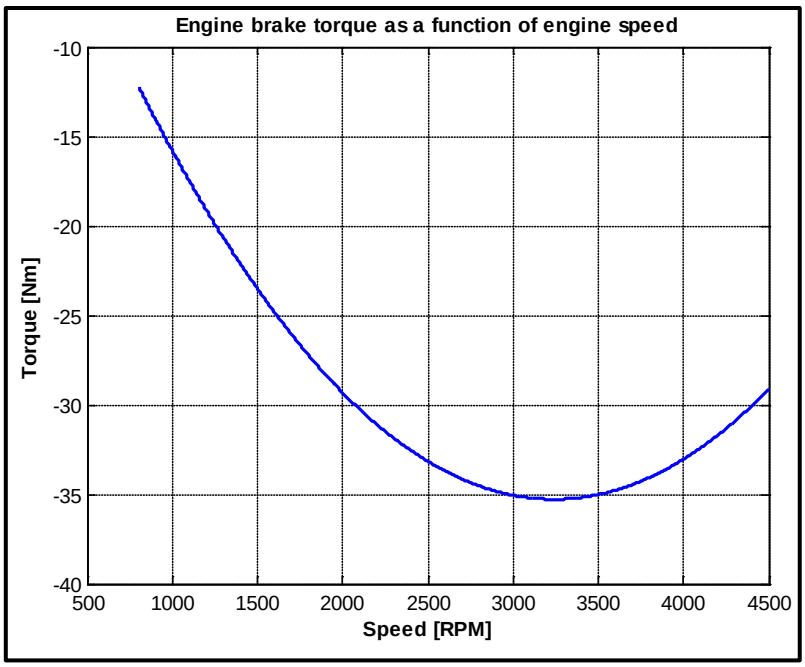

Figure 2. 14 – Engine braking torque as a function of engine speed

2.5.4 Brakes

The brakes were characterised as a relationship between the brake line pressure and the longitudinal deceleration measured with an accelerometer. The brakes were characterised by accelerating the vehicle to 70km/h and then braking to standstill while measuring the longitudinal acceleration and the brake line hydraulic pressure. Figure 2.15 shows that a linear relationship (given by Equation (2.8)) exists between brake line pressure and deceleration. Multiplying the deceleration with the vehicle mass gives the braking force.

$$A_{Brakes} = 0.546 P_{hyd} - 0.3713 \quad (2.8)$$

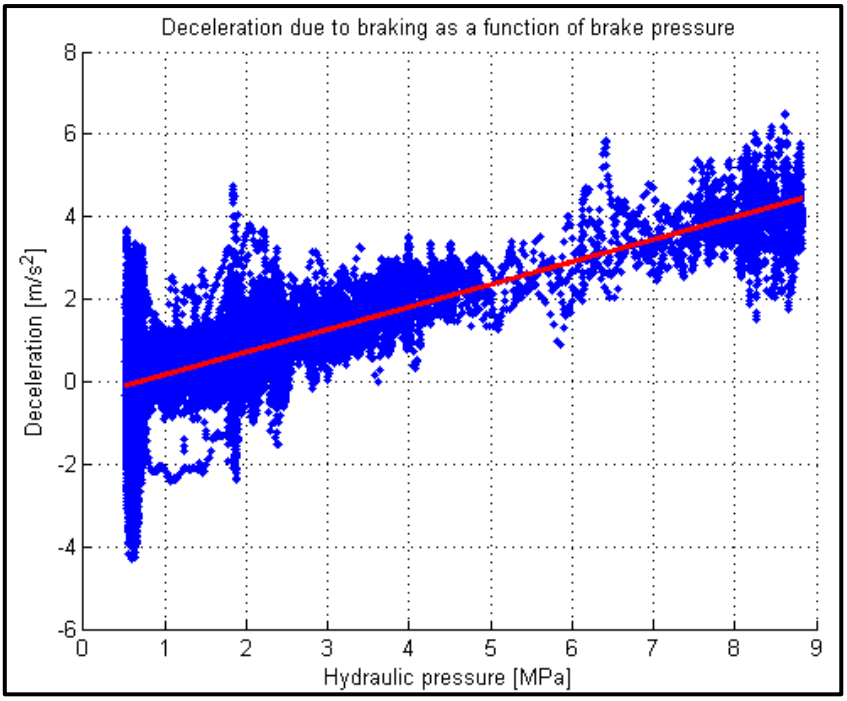

Figure 2.15 – Longitudinal deceleration as a function of brake line hydraulic pressure

2.5.5 Updating and validating the mathematical model

The relationships developed in Section 2.5.1 had to be incorporated in the MSC.ADAMS/View and Simulink model of the Land Rover Defender. Figure 2.16 shows a block diagram of the longitudinal model of the Land Rover. Note that the engine braking torque is included in the Engine Map block in Figure 2.16. The variables measured from the MSC.ADAMS/View model are vehicle speed and driveshaft speed. The control inputs given are the throttle position, brake line pressure and the gear selected. These measured variables and control inputs are used to determine the driveshaft torque (i.e. supply force) and demand force acting on the vehicle.

A validation run was done with the Land Rover Defender while recording the vehicle's speed, throttle pedal position, brake line hydraulic pressure and clutch pedal position. The validation run consisted of four stages (see Figure 2.17):

1. Accelerating from a standing start in first, second and third gear to 60km/h (from 0 to approximately 15s).
2. Decelerating by coasting in third gear from 60km/h back to idle speed (from approximately 15s to just before 30s).
3. Accelerating in third and fourth gear from third gear idle speed up to 90km/h (from 30s to approximately 55s).
4. Braking with the clutch disengaged (from 55s onwards).

The measured throttle pedal position and brake line pressure were used as inputs to the mathematical model. The gear change timing was accomplished by manually selecting the time

(using MATLAB's 'ginput' function) at which the clutch pedal was depressed and incrementing the gear selection at each point.

The resulting speed, as calculated by the model is compared with the measured speed in Figure 2.17. Figure 2.18 shows the torque applied to the driveshaft during the validation run. As may be seen in Figure 2.17, there are some discrepancies present when comparing the modelled speed and measured speed of the vehicle. These errors may be attributed to:

1. Inaccurate gear change timing
2. The validation run was conducted on a slight downhill and the model does not provide for the effect of the component of gravity along an incline (although Equation (2.4) provides for the force component due to longitudinal inclination but it was not implemented in the model due to the difficulties in measuring the incline of the test track).
3. There may have been external contributing factors (such as wind loading) that were not measured and not accounted for in the model.

However, despite these discrepancies, a very close correlation may be seen in Figure 2.17, which was deemed acceptable for the purposes of this investigation.

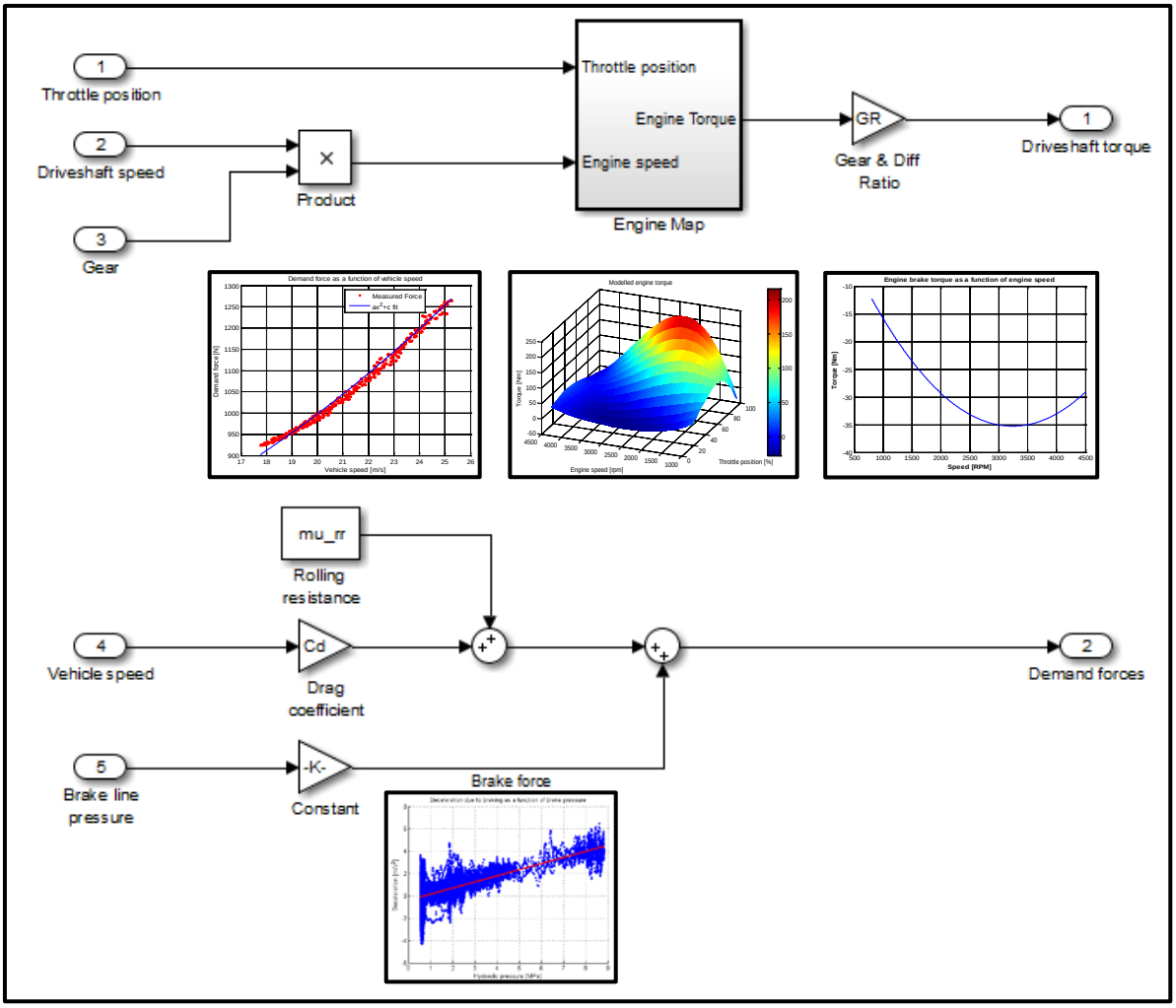

Figure 2.16 – Schematic layout of mathematical longitudinal model of the Land Rover

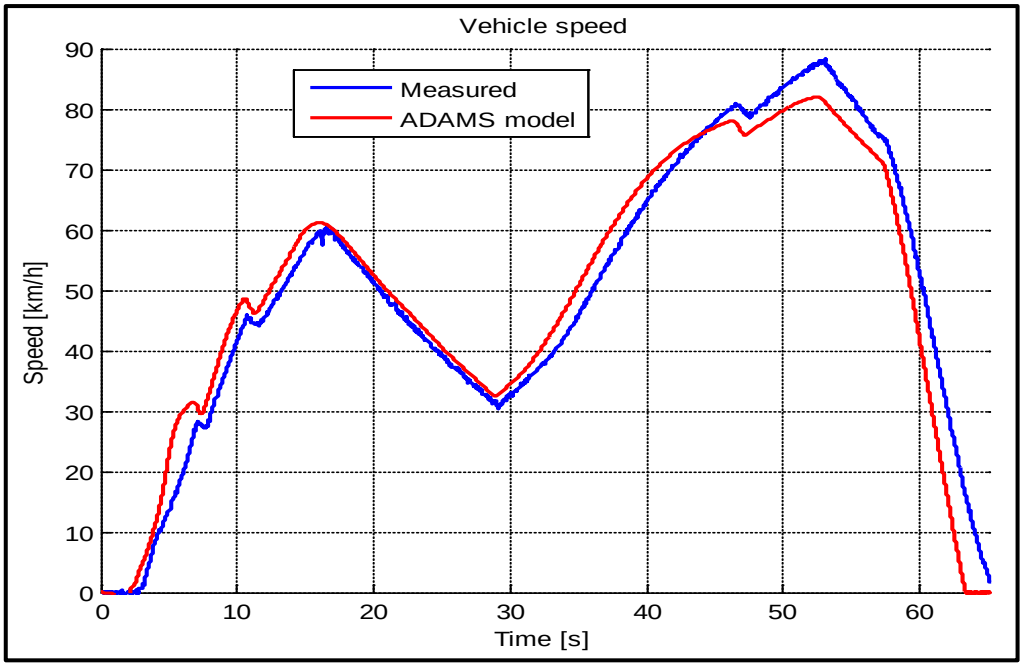

Figure 2.17 – Comparison of measured and modelled vehicle speeds for the validation run

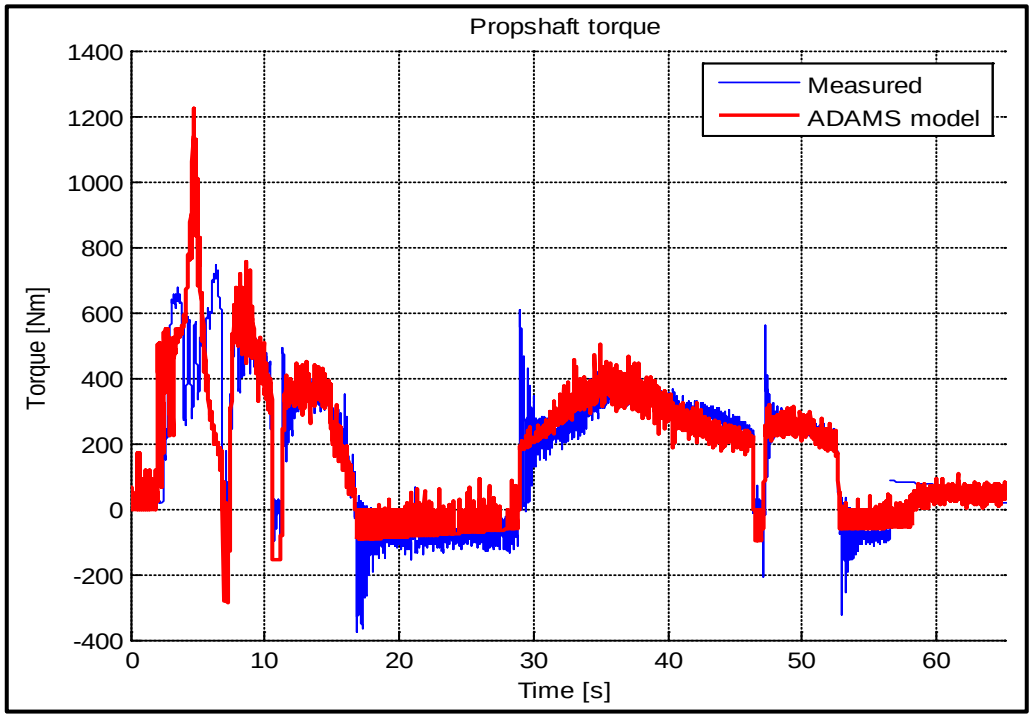

Figure 2.18 – Measured and modelled driveshaft torque for the validation run

2.6 Conclusion

The aim at the start of this chapter was to expand the existing MSC.ADAMS/View and Simulink model of the Land Rover Defender. The existing model provided for validated simulation of the lateral and vertical dynamics of the Land Rover Defender, but lacked the longitudinal dynamics associated with supply and demand forces acting on the vehicle. (To aid in the repeatability of characterisation tests, the throttle pedal actuator was improved.)

Expansion of the MSC.ADAMS/View and Simulink model required modelling of the following subsystems:

- The engine map, which was modelled as a function of engine speed and throttle pedal position using a three dimensional polynomial fit.
- The demand forces acting on the vehicle due to aerodynamic drag and rolling resistance.
- The longitudinal deceleration of the vehicle as a function of the hydraulic pressure in the brake lines, modelled using a straight line relationship.
- The engine braking torque as a function of the engine speed with a parabolic curve.

The expanded MSC.ADAMS/View model of the Land Rover Defender was validated by comparing the measured vehicle speed to the modelled vehicle speed for a validation test run. The measured torque applied to the driveshaft during the validation run was also compared to the torque predicted by the model. In both cases a very close correlation was seen and the longitudinal dynamics of the MSC.ADAMS/View model of the Land Rover was deemed to be validated. Simulation results predicted by the MSC.ADAMS/View model may thus be trusted.

The inputs required by the expanded MSC.ADAMS/View and Simulink model of the Land Rover Defender are the same as the inputs given by the actuators that will be used for autonomous control. The MSC.ADAMS/View model may thus be used in conjunction with an autonomous control system that generates the inputs required by the autonomous control actuators. The existing models of these actuators may then be used to generate the inputs to the MSC.ADAMS/View model.

The model is now ready to be used in the development of the longitudinal control system.

Chapter 3

The longitudinal control system

I cannot always control what goes on outside, but I can always control what goes on inside

– Wayne Dyer (1940-) Self-help author and motivational speaker

3.1 Introduction

The aim of the autonomous longitudinal control system to be implemented on the Land Rover test vehicle is to improve the vehicle's safety by controlling the vehicle's longitudinal behaviour. A common problem with sports-utility-vehicles is the low rollover threshold, due to a high centre of gravity. The rollover threshold is given by Equation (3.1) (Gillespie 1992: 311):

$$\frac{A_y}{g} = \frac{t_w}{2h} \tag{3.1}$$

Several methods of increasing the rollover threshold may be identified when investigating Equation (3.1), such as lowering the centre of gravity or increasing the vehicle's track width. These, however, require extensive mechanical modifications to the vehicle. The lateral acceleration experienced by a vehicle when negotiating a corner is given by Equation (3.2) (Gillespie 1992: 198). Equation (3.2) is derived for steady-state cornering (where the vehicle is traveling at a constant speed on a curve with constant radius). The method of reducing the vehicle's rollover propensity to be investigated by this project is to reduce the lateral acceleration experienced by the vehicle by reducing the maximum speed or increasing the turn radius, rather than changing the rollover threshold.

$$A_y = \frac{V^2}{R} \tag{3.2}$$

From Equation (3.2) it may be seen that by increasing the radius of the corner being negotiated, the lateral acceleration will be reduced and the speed at which rollover will occur is correspondingly increased, hence the development of a trajectory planning algorithm that maximises the radius of curvature. Although Equation (3.2) is developed for steady-state cornering – which may not necessarily be the case during driving – it was assumed that the use of Equation (3.2) is sufficient for the purpose of this investigation. The use of an optimisation algorithm to determine the minimum curvature may also result in a "smoother" route, reducing the effect of transient cornering. The method described in Section 3.3.1 to determine the radius

of the trajectory also fits a curve with constant radius through three consecutive points of the prescribed path which also allows the use of the steady-state lateral acceleration for simplification purposes.

From the trajectory planning algorithm, a reference vehicle speed will be developed to keep the lateral and longitudinal acceleration within prescribed boundaries. The reference vehicle speed will take into account the friction available for force generation by the tyres in both the longitudinal and lateral directions (i.e. the friction circle) and the limits imposed by the vehicle's dynamic performance. A control algorithm that tracks the reference speed by generating inputs to the Land Rover test vehicle (the throttle position, brake line pressure and gear selection), so that it follows the reference speed as determined with the trajectory planning algorithm, will then be developed. This algorithm will be tested first with the MSC.ADAMS/View model of the vehicle before being implemented on the vehicle itself.

3.2 Trajectory planning

The roads or tracks used for simulation and experimental purposes are defined using GPS coordinates (lateral and longitudinal), which can be converted to *x* and *y* coordinates of the road centreline. By specifying the road width, the road boundaries may also be determined. Trajectory planning is concerned with determining the path the vehicle must follow when negotiating a specified road or track. The trajectory may be optimised for various operating conditions. Braghin *et al.* (2011) developed two such methods – optimising for the shortest route and optimising for the minimum curvature, as described in paragraph 1.2.3. The minimum curvature formulation is applicable for the case under investigation, wherein minimising the curvature of the path followed by the vehicle will result in maximizing the radius of the trajectory and hence lowering the lateral acceleration (see Equation (3.2)).

The minimum curvature formulation developed by Braghin *et al* (2011), which relies on fitting closed 'natural' splines through the proposed points on the trajectory, was modified to rather make use of finite difference methods. When considering curvature, one has to consider arc length too (Stewart 2003: 862). To determine the curvature of an arc (in this case the trajectory), the *x* and *y* coordinates are parameterised with respect to a free variable *r*. The arc length *s* is then determined by Equation (3.3) (Stewart 2003: 863):

$$s(r) = \int \sqrt{\left(\frac{dx}{dr}\right)^2 + \left(\frac{dy}{dr}\right)^2} \tag{3.3}$$

The curvature of an arc is then given by (Stewart 2003: 864)

$$\kappa^2 = \left(\frac{d^2x}{ds^2}\right)^2 + \left(\frac{d^2y}{ds^2}\right)^2 \tag{3.4}$$

This approach, however, is based on piece-wise smoothly defined functions, which is not the case for this study. Since the road paths consist of discrete points of which only the *x* and *y*

coordinates are known, numerical approximation has to be used to differentiate the path to find the curvature and hence the use of finite difference methods.

To determine the arc length, Pythagoras's theorem is used to calculate the distance of each track segment (Equation (3.5)). The forward difference method is then used to determine the second derivatives of the trajectory. The forward difference formula for second order differentiation is given by Equation (3.6) (Burden and Faires, 2005).

$$\Delta s_i = \sqrt{\Delta x_i^2 + \Delta y_i^2} \tag{3.5}$$

$$f''(x) = \frac{1}{h^2}[f(x) - 2f(x+h) + f(x+2h)] \tag{3.6}$$

Recalling Equation (1.5) that defines the vehicle's position on the road relative to the road boundaries (Equation (1.5) is repeated here as Equation (3.7) for the sake of continuity) and applying Equation (3.6) to the first term in Equation (3.4) results in:

$$P = x_r + \alpha(x_l - x_r)\hat{\boldsymbol{\imath}} + y_r + \alpha(y_l - y_r)\hat{\boldsymbol{\jmath}} \tag{3.7}$$

$$\frac{d^2x_i}{ds^2} \approx \frac{1}{\Delta s_i^2}\left[x_{r,i+2} - 2x_{r,i+1} + x_{r,i} + \langle \Delta x_{i+2} \quad -2\Delta x_{i+1} \quad \Delta x_i \rangle \begin{Bmatrix} \alpha_{i+2} \\ \alpha_{i+1} \\ \alpha_i \end{Bmatrix}\right] \tag{3.8}$$

A similar Equation may be formulated for the $\frac{d^2y_i}{ds^2}$ term in Equation (3.4). Using these Equations in Equation (3.4) and summing for each track segment results once again in the standard quadratic form (this time, however, for the minimum curvature formulation (Rao 2009: 230)):

$$\kappa^2 = \frac{1}{2}\langle \alpha_\kappa \rangle [H_\kappa] \{\alpha_\kappa\} + \langle B_\kappa \rangle \{\alpha_\kappa\} \tag{3.9}$$

Using MATLAB's quadratic optimisation function, the trajectory's curvature is minimised. Figure 3.1 shows the trajectory as optimised for Gerotek's ride and handling track (Gerotek Test Facilities)

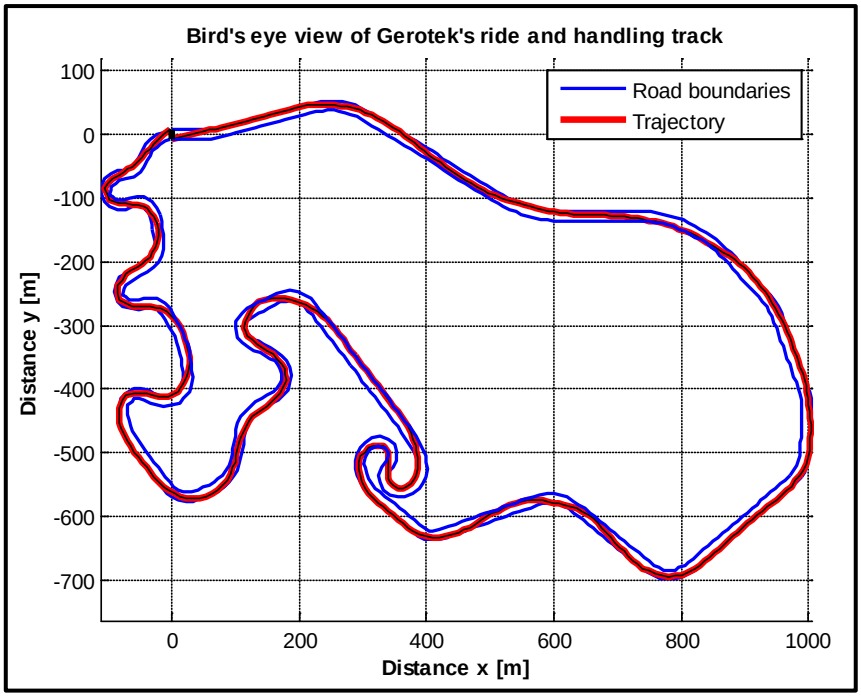

Figure 3.1 – Minimised curvature trajectory of Gerotek's ride and handling track (Gerotek Test Facilities)

3.3 Speed profile

Once the minimum curvature trajectory has been determined, a reference speed at which the vehicle will attempt to negotiate the track must be determined. This speed is limited by three factors, namely:

- the lateral acceleration limit,
- the friction limit when longitudinal and lateral acceleration is present (combined loading) and
- the vehicle's limitations with regards to longitudinal acceleration and deceleration.

The process followed to formulate the speed profile is given schematically in Figure 3.2.

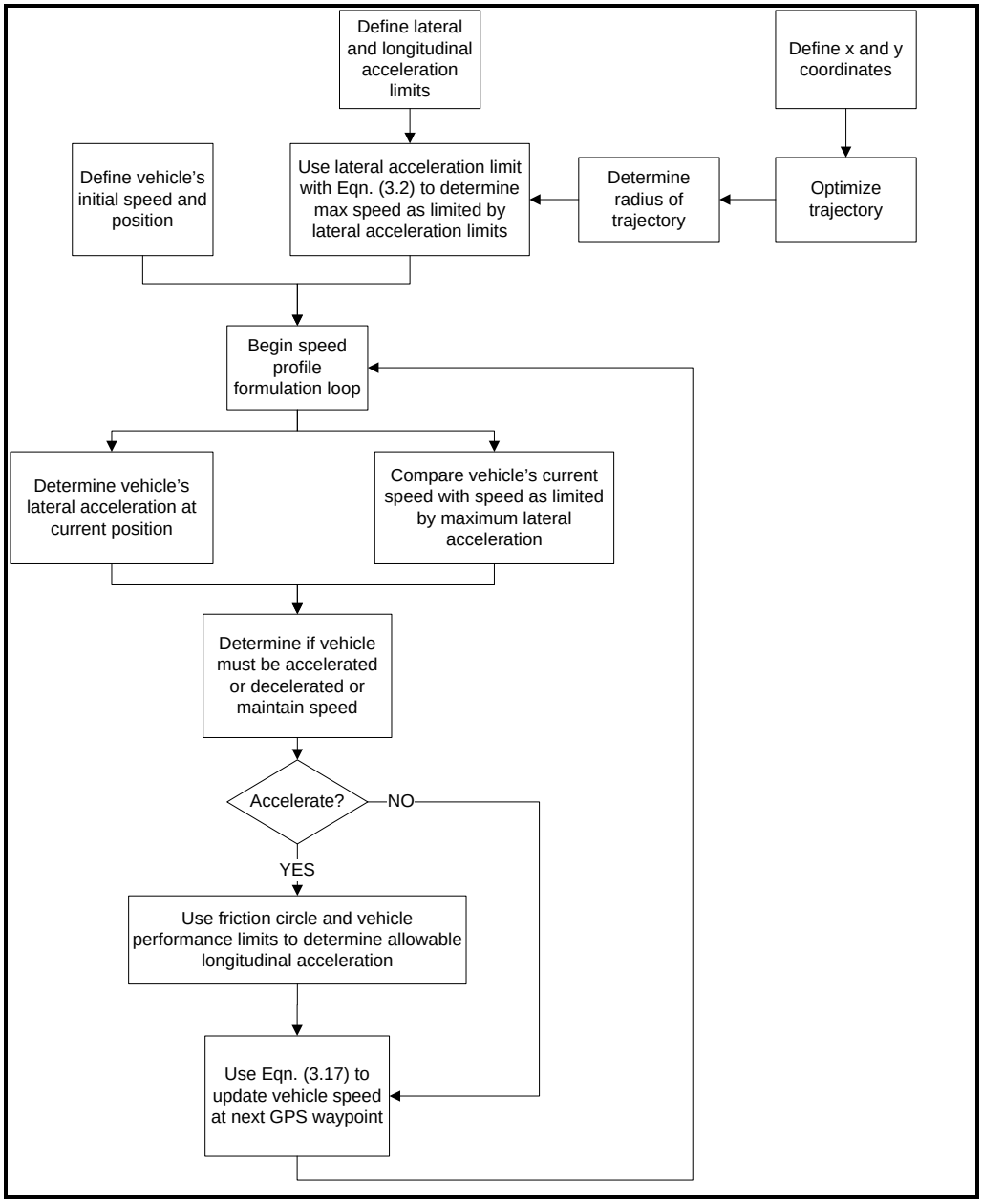

Figure 3.2 – Flowchart describing formulation of speed profile

3.3.1 Speed limit due to lateral acceleration

As is evident in Equation (3.2), the speed limit due to lateral acceleration is a function of the radius of the trajectory being followed. The radius of a curve is given by Stewart (2003: 867) as being the inverse of curvature. This would indicate that the curvature determined in Section 3.2 may be used to determine the radius. However, the method of formulating the curvature in Section 3.2 disregards the constant term (this would have no effect on the optimisation algorithm (Rao 2009: 1)) and is thus not representative of the actual curvature. For this reason, an algorithm for determining the radius of the trajectory for each segment of the trajectory was developed. Given three points, it is always possible to draw an arc with a constant radius that

passes through all three points. The perpendicular bisectors of the chords joining adjacent points pass through the centre of the arc. The distance from the centre of the arc to any of the three points used is the radius of curvature. Figure 3.3 shows the result of this procedure.

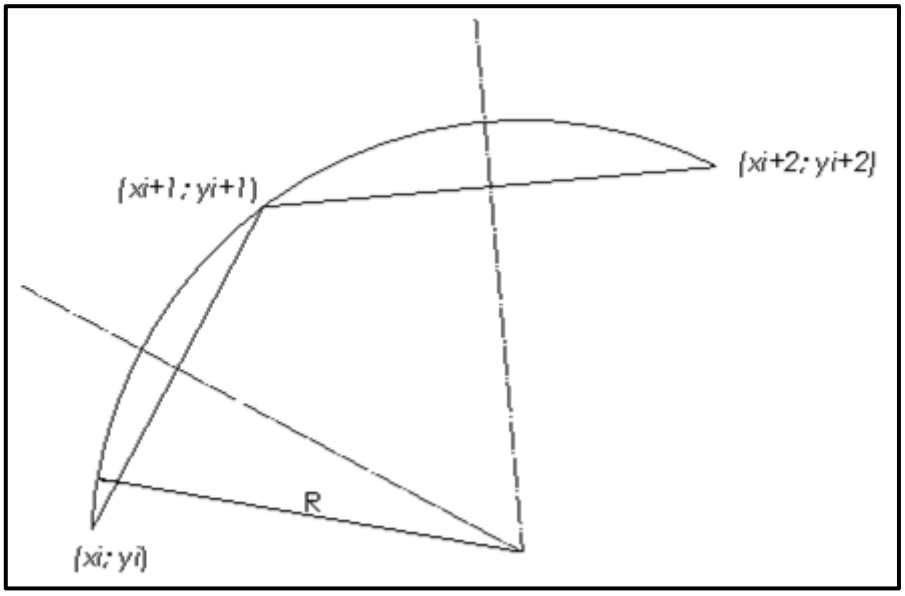

Figure 3.3 – Constructing an arc through three points

The mathematical operations needed to determine the radius of curvature following this procedure will now be explained. First, the perpendicular bisectors are determined. The bisectors are located at the centre of each chord, thus the centre points of each chord have to be determined:

$$x_{q,i} = \frac{1}{2}(x_i + x_{i+1}) \tag{3.10}$$

$$y_{q,i} = \frac{1}{2}(y_i + y_{i+1}) \tag{3.11}$$

The line bisecting the chord from the two adjacent points is perpendicular to the chord, hence the product of the chord and the bisector must equal negative one. The gradient of the chord is thus determined and used to determine the gradient of the bisector:

$$m_i = \frac{\Delta y_i}{\Delta x_i} = \frac{y_{i+1} - y_i}{x_{i+1} - x_i} \tag{3.12}$$

The bisector's gradient is given by equation (3.13):

$$m'_i = \frac{-1}{m_i} \tag{3.13}$$

Finally the constant term describing the straight line equation of the bisector is determined. Since it is known that the bisector passes through the point $(x_{q,i}; y_{q,i})$, the constant term is calculated with:

$$c_i = y_{q,i} - m'_i x_{q,i} \tag{3.14}$$

The centre point of the arc is then at the intersection of the two bisectors, given by Equation (3.15) and (3.16):

$$x_{R,i} = \frac{c_{i+1} - c_i}{m'_i - m'_{i+1}} \tag{3.15}$$

$$y_{R,i} = m'_i x_{R,i} + c_i \tag{3.16}$$

The radius of the arc (and hence the radius of curvature) is then determined with Pythagoras' theorem:

$$R_i = \sqrt{\left(x_{R,i} - x_i\right)^2 + \left(y_{R,i} - y_i\right)^2} \tag{3.17}$$

Figure 3.4 shows a spiral with a radius increasing from zero to 50m. The radius of curvature is confirmed with the outlined algorithm. The radius as a function of arc length is also shown in Figure 3.4. A slight discrepancy between the true and calculated radius may be seen in Figure 3.4. This discrepancy is present right at the beginning of the spiral. A possible explanation is that the algorithm cannot calculate a radius of zero. The algorithm works well for radii greater than five meter and is thus more than adequate for vehicle trajectory, since a vehicle's turning radius is seldom less than five meter.

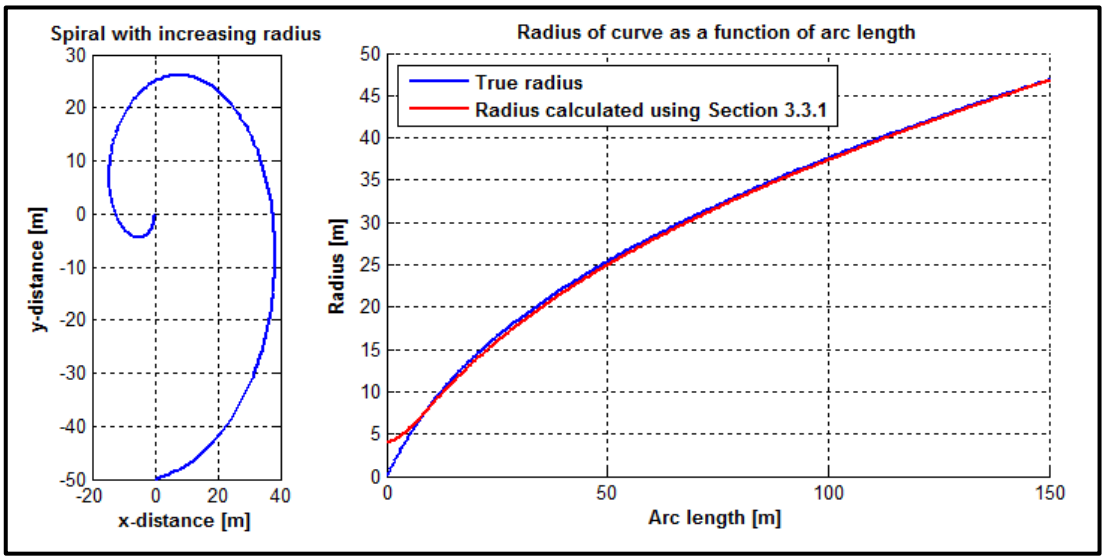

Figure 3.4 – Spiral with radius increasing from zero to 50m and radius as a function of arc length

This algorithm may now be used to determine the maximum permissible speed for the vehicle around any racetrack. By specifying a maximum lateral acceleration, the corresponding speed at which this acceleration will occur may be calculated for each point on the trajectory. However, from Equation (3.2) it may be seen that when the radius of the trajectory is large, the permissible speed is very high (in a straight line, there is no lateral acceleration) and hence a speed limit of 130km/h was imposed. This is approximately the maximum speed the Land Rover can achieve. Figure 3.5 shows the speed as limited by lateral acceleration for the Land Rover around the Gerotek ride and handling track. A maximum lateral acceleration of 0.5g was specified.

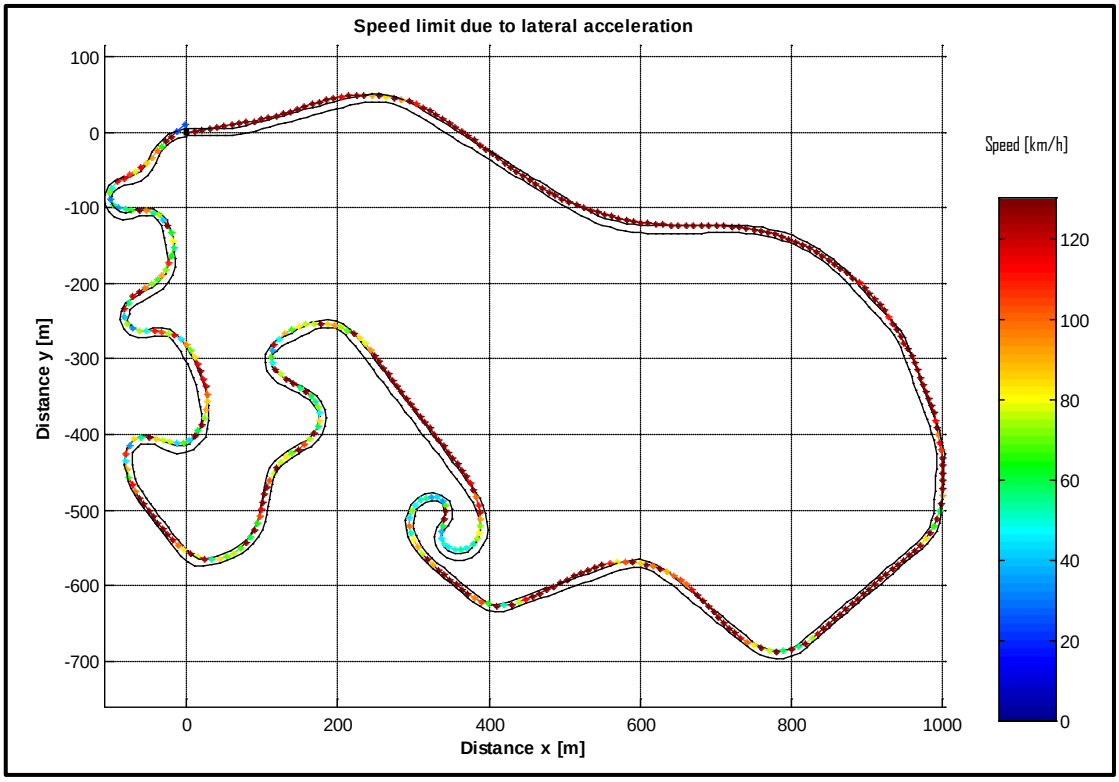

Figure 3.5 – Speed limit due to lateral acceleration for the Land Rover at Gerotek's ride and handling track (maximum lateral acceleration of 0.5g and top speed limited to 130km/h)

3.3.2 Speed limit due to friction and vehicle performance

When accelerating a vehicle both longitudinally and laterally simultaneously, one has to consider the friction circle. Since forces are being generated in two directions in a highly nonlinear system, one cannot simply consider each load condition separately. In Section 3.3.1 the speed profile around the track was optimised for maximum lateral acceleration and hence maximum force generation. However, there are certain sections along the track where the maximum lateral force is not reached (due to the vehicle's limitations). In these conditions there is thus some friction force available for longitudinal acceleration or deceleration. This available friction thus limits the vehicle's longitudinal performance (if the friction force is exceeded, the wheels would slip (spin or lock), which may result in an unstable and unsafe situation).

The friction available for longitudinal acceleration is thus governed by the friction circle. As discussed in Chapter 1, the friction force available for longitudinal acceleration is the vector subtraction of the developed lateral force from the friction force limit. This is determined with Equation (3.18) (Braghin *et al* (2011)):

$$A_{x,i} = A_{x,max}\sqrt{1 - \left(A_{y,i}/A_{y,max}\right)^2} \tag{3.18}$$

By imposing a speed limit on the vehicle when negotiating the track, the maximum longitudinal acceleration allowable may be determined. Considering the vehicle's limitations in terms of performance and braking, one may determine the distance required to accelerate and decelerate the vehicle. The vehicle's performance capabilities on a level road are shown as functions of vehicle speed in Figure 3.6. These plots were determined from the experimental data, discussed in detail in Chapter 2.

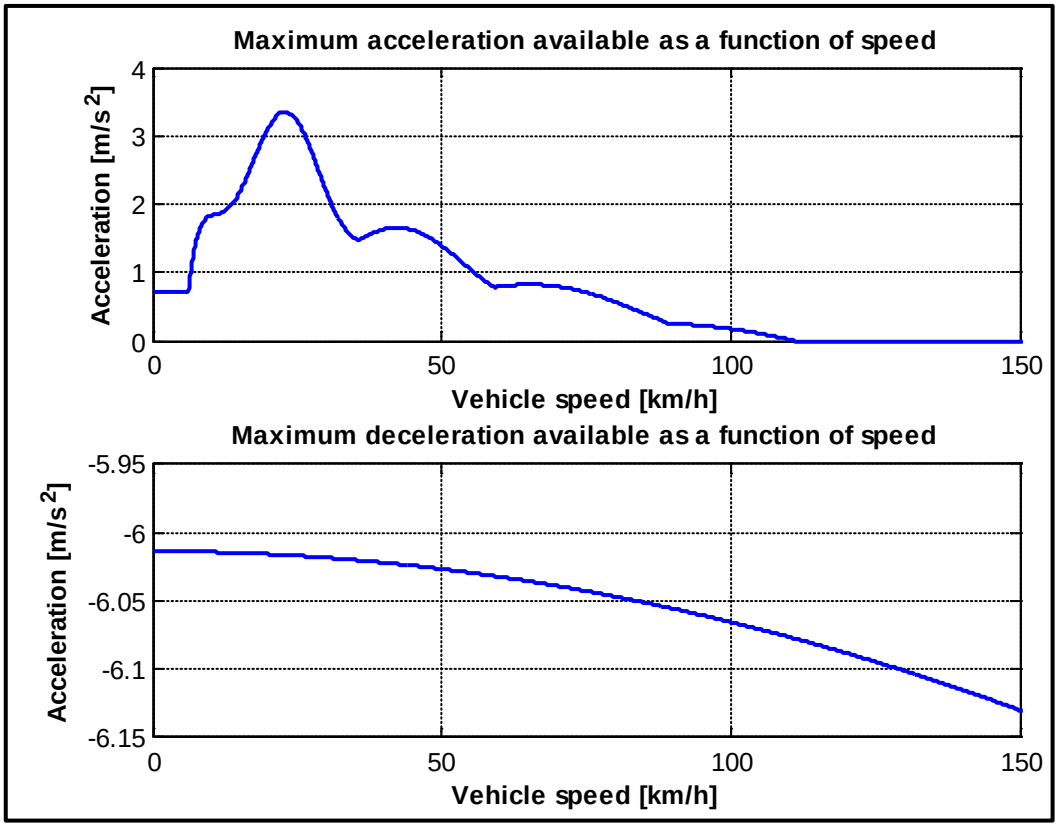

Figure 3.6 – Land Rover performance limits

3.3.3 Speed profile algorithm

The speed profile that will be used as the reference speed to be maintained by the vehicle while negotiating the prescribed path is then determined by defining the maximum lateral and longitudinal acceleration deemed safe. A preview distance is defined as a function of the current vehicle speed and the maximum allowable longitudinal acceleration; the function is given in Equation (3.19).

$$d_{prev} = V\tau - 0.5A_{maxlong}\tau^2 + const \qquad (3.19)$$

The minimum speed as limited by the lateral acceleration of the vehicle (see Equation (3.2)) for the path to be followed from the current position to the preview point is compared with the current speed of the vehicle. If the minimum speed is greater than the current vehicle speed, the vehicle is allowed to accelerate. The acceleration allowed is determined by comparing the vehicle's performance capability (see Figure 3.6) and the friction available at the current position (see Equation 3.18). The lesser of these two accelerations is used for the desired longitudinal

acceleration. The vehicle's speed at the next position in the path is then updated using the equations of motion assuming constant acceleration (see Equation (3.20)):

$$V_{i+1} = \sqrt{V_i^2 + 2A_x \Delta s_i} \tag{3.20}$$

3.3.4 Discussion of speed profile algorithm results

Figure 3.7 shows the reference speed for Gerotek's ride and handling track. The red line is the speed limit imposed by Equation (3.2) and the blue line the reference speed calculated with Equation (3.20). It may be noted that the blue line is never higher than the red line, indicating that, if the control system tracks the reference speed accurately, the vehicle will never exceed its lateral limits due to excessive speed. This is validated in Section 3.4.

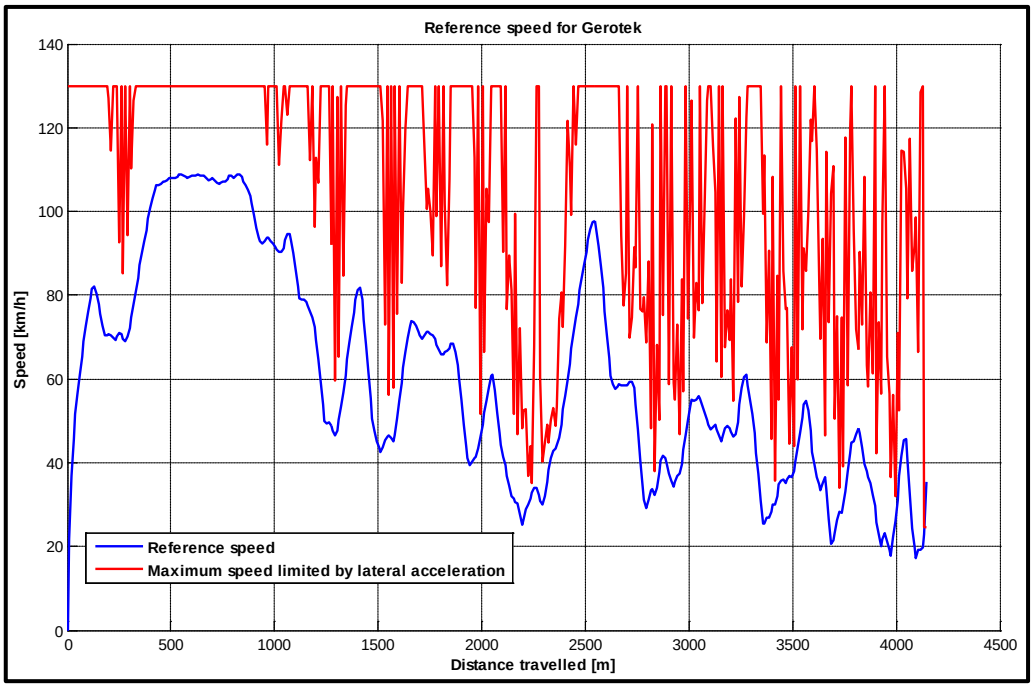

Figure 3.7 – Reference speed for Gerotek's ride and handling track

While the approach followed above worked for the case study of Gerotek's ride and handling track (Gerotek Test Facilities), some extreme cases may occur when the vehicle may exceed the lateral acceleration target. An example of such a case is when the vehicle is negotiating a long curve with constant radius. Since the curve is long, the vehicle is allowed to increase speed until it reaches the lateral acceleration target. If the lateral acceleration target is set at the vehicle's physical limit, the vehicle will not be able to reduce speed (due to the fact that no friction is available for deceleration) for an upcoming curve with a smaller radius (where a lower speed is necessary). An improved approach would be to iteratively solve Equations (3.19) and (3.20) to ensure that such a situation never occurs. This however requires *a priori* knowledge of the path that is going to be driven. While the route is known beforehand when one is conducting simulations or even applying this algorithm to racing situations where the vehicle will be negotiating a predetermined racetrack or route, this is not practically feasible when applied to vehicles used for everyday driving on public roads. *A priori* knowledge of the route would allow

one to determine the speed profile starting at the end of the route and working ones way to the start without ever encountering such a dangerous situation. Setting the lateral acceleration targets to be at the same value as the vehicle's limit however defeats the purpose of implementing a speed limiting driver assist system in the first place. For practical implementation the acceleration targets should typically be set to a value that is 70 to 80% of the vehicle's limit in which case a safety margin will be available for braking. The proposed algorithm may not be ideal, but considering the guidelines used for road construction and the speed limits imposed on public roads, the probability of encountering such a situation is small.

3.4 ADAMS validation of control system

The reference speed profile developed in Section 3.3.3 had to be validated before implementation on the actual test vehicle could commence. For this purpose, the MSC.ADAMS/View model, as developed in Chapter 2 is used. Before simulation could start, some basic control strategies had to be developed to control the actuator positions. These control strategies control:

- the throttle pedal position,
- the brake line hydraulic pressure and
- the gear selection.

The throttle pedal position was controlled with a PID controller and the brake pedal with a PI controller. The cumulative errors were set to zero each time the control system switched modes (accelerating and braking). The equation for a PID controller is (Dorf and Bishop 2008: 444):

$$u(t) = K_P e(t) + K_I \int e(t)dt + K_D \frac{de(t)}{dt} \qquad (3.21)$$

The equation for the PI controller is similar to Equation (3.21), with the derivative gain K_D set to zero. The gains used for the PID and PI controller are given in Table 3.1. Due to the nonlinear nature of the Land Rover model it was not possible to determine these gains in an optimal way (as would have been the case if the model was linear and techniques such as the root locus method could be used (Dorf and Bishop 2008: 407-492)). The gains were thus determined with a trial-and-error approach. The throttle pedal position was limited between 0 and 100% throttle and the brake pressure was limited between 0 and 10MPa.

Table 3. 1 – Throttle pedal position and brake pressure controller gains

Throttle pedal position controller		Brake pressure controller	
Gain	Value	Gain	Value
K_P	20	K_P	2
K_I	200	K_I	100
K_D	15		

The velocity error is determined with Equation (3.22), with the control system distinguishing between a positive and a negative error to determine whether acceleration or deceleration of the vehicle is necessary. When the error causes the vehicle to brake, the throttle position is immediately set to zero and vice versa. The control signals sent to the vehicle are the throttle pedal position and brake line hydraulic pressure.

$$e = V_{ref} - V \tag{3.22}$$

The gear selection is simply done by monitoring the engine speed. If the engine speed is higher than 3500 RPM the gear is incremented once (unless the vehicle is in top gear) and if the engine speed is less than 1200 RPM the gear is decremented once (unless the vehicle is in first gear). Although this is not an optimum gear shifting regime (the ideal would be to change gears at the intersection of the supply curves in the various gears on a supply force vs. vehicle speed graph), this method of controlling the gear selection was chosen due to its simplicity and the ease with which such a feedback control system could be implemented on the actual test vehicle.

The next step was to simulate the MSC.ADAMS/View model of the Land Rover's response to the inputs generated by the developed control system (which tracks the reference speed profile formulated in Section 3.3.3). The results for several racetracks of which the GPS waypoints were available (obtained from Racelogic's website) are shown in Figures 3.8 to 3.10. It was assumed throughout that these racetracks were flat, since no elevation data was available. Figures 3.8 to 3.10 show the trajectory followed by the vehicle around the track, the vehicle's speed along with the reference speed and a g-g diagram of all the points along the track.

It may be seen in Figures 3.8 to 3.10 that the formulated speed profile (the reference speed, or red line in the centre graph) stays below the speed as limited by Equation (3.2) – the speed limited by Equation (3.2) is the green line in the centre graph. The speed that the model of the vehicle attained during simulation is shown as the blue line in the centre graph. It may be noted that the simulated speed never exceeds the speed profile and that it tracks the prescribed speed closely. The resultant longitudinal and lateral accelerations are plotted in the bottom graph and the top right g-g diagram. The g-g diagrams in Figures 3.8 to 3.10 indicate that the vehicle largely stayed within the prescribed acceleration boundaries (the red circle is the friction circle with longitudinal and lateral acceleration limits of 8m/s^2). The occasions when the vehicle exceeded the set acceleration boundaries may be attributed to path following errors. The driver model used during the simulations maintained control over the vehicle at all times, even though the prescribed acceleration boundaries are very close to the vehicle's limits.

In Figures 3.8 to 3.10 it may be seen that there is a discrepancy between the simulated vehicle speed (the blue line) and the reference speed (the red line) during forward acceleration. This is because the algorithm to determine the maximum forward acceleration was biased to favour the

friction limit rather than the vehicle's performance limit. This was done because of the extremely nonlinear characteristic of the vehicle's forward performance capability. When calculating the reference speed at the next step with Equation (3.20), the assumption of constant acceleration is made. While the vehicle's deceleration is approximately constant under braking, this is not the case for forward acceleration. Although the reference speed may then accelerate faster than the vehicle is capable, the vehicle's acceleration in the model is limited by the engine performance as modelled in Section 2.5.1. It may be seen that throughout all the simulations the vehicle accurately tracked the reference speed when braking.

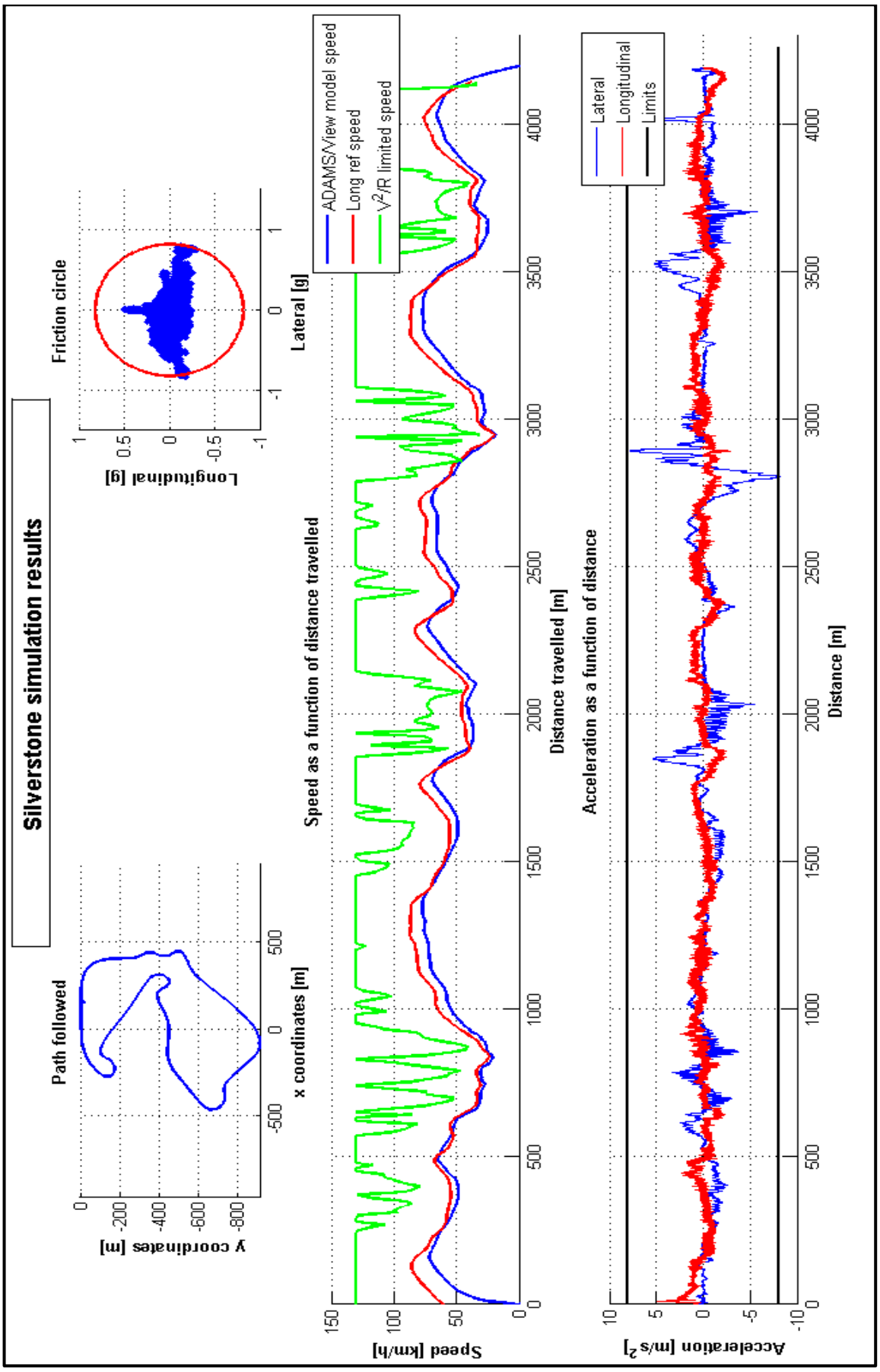

Figure 3.8 – Simulation results for Silverstone (maximum lateral and longitudinal acceleration of 8m/s^2)

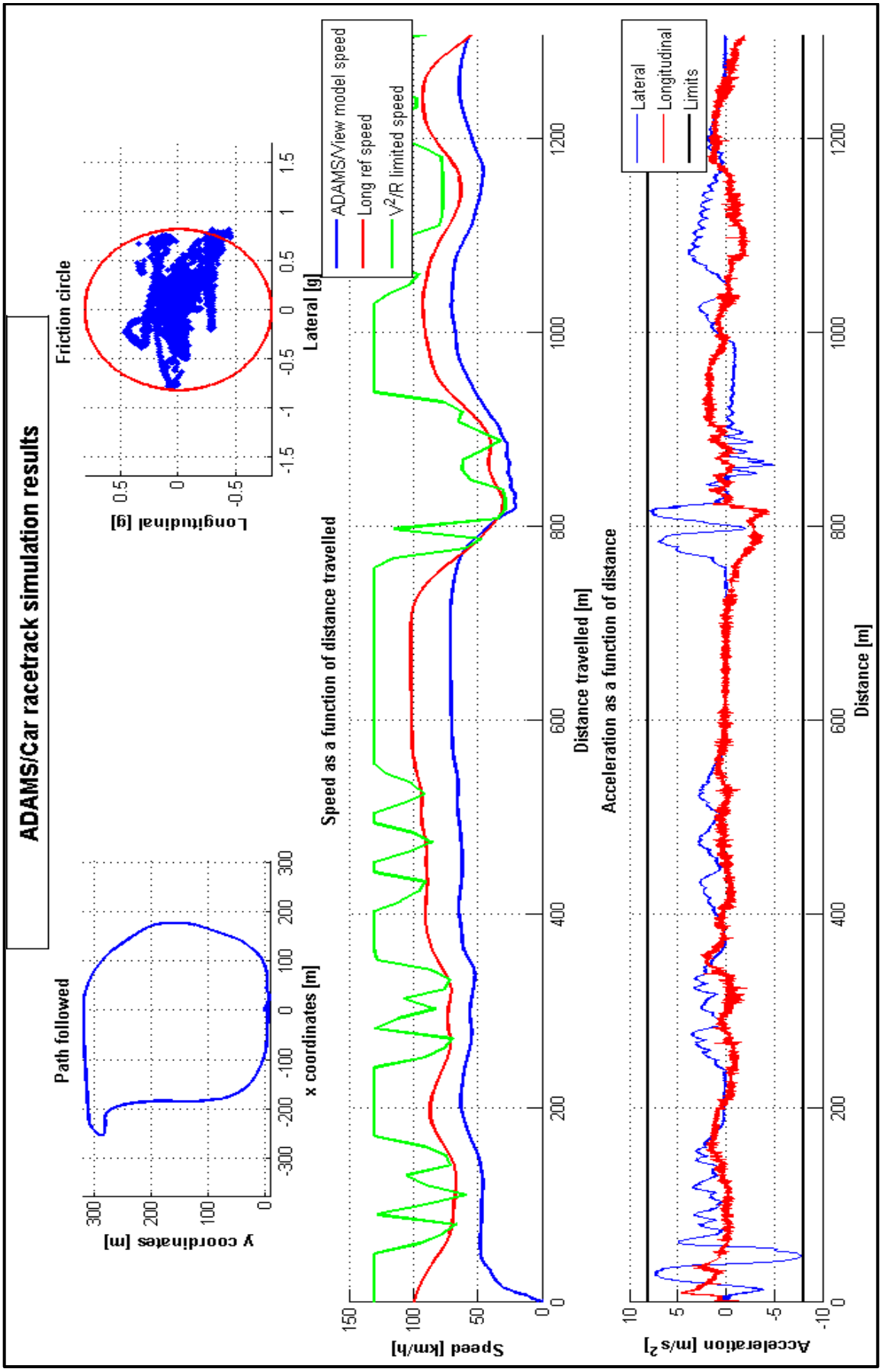

Figure 3.9 – Simulation results for ADAMS/Car racetrack (maximum lateral and longitudinal acceleration of 8m/s^2)

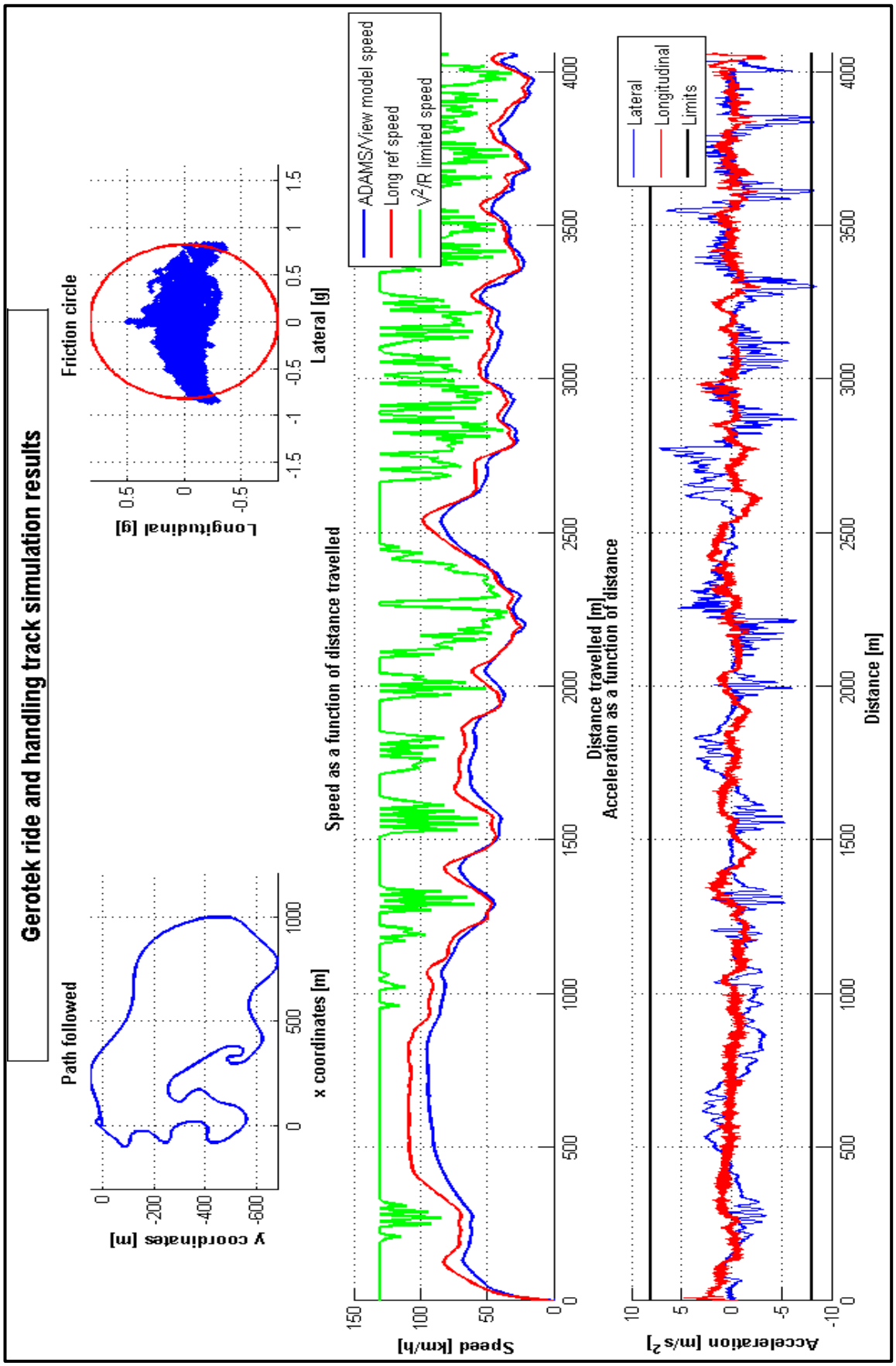

Figure 3.10 – Simulation results for Gerotek's ride and handling track (maximum lateral and longitudinal acceleration of 8m/s^2)

3.5 Conclusion

The development of a control system that controls the Land Rover test vehicle's longitudinal performance was motivated by the limited lateral performance capabilities of sports-utility-vehicles. Generally, these vehicles have a very low roll over threshold due to their high centre of gravity. Several mechanical improvements are possible that may increase the roll over threshold, but these methods would entail large modifications to existing experimental vehicle. Rather than modifying the vehicle's dimensions, an algorithm to determine the maximum speed at which the vehicle can safely negotiate a prescribed path was developed.

This speed profile algorithm considers the following parameters:

- The trajectory of the prescribed path (in terms of x and y coordinates)
- The speed limit due to lateral acceleration limitations.
- The limits imposed on the system by the limited friction available for force generation.

By maximising the radius of curvature of the trajectory of the vehicle through a series of corners (such as around a racetrack or over a mountain pass) the maximum speed at which the vehicle can negotiate the corners safely can be increased. Such a trajectory planning method, developed from work done by Braghin *et al* (2011) was implemented. The 'optimum' path was thus determined and from this path a maximum speed as limited by the maximum lateral acceleration the vehicle can achieve was determined with Equation (3.2). At this speed, maximum lateral force is being generated by the tyres and there is no possibility of generating any longitudinal force. However, when the trajectory has no curvature and since the lateral acceleration is inversely related to the radius of curvature, the speed limit is infinite. By imposing a maximum speed of 130 km/h (this correlates with the maximum theoretical speed of the vehicle), a suitable or safe speed profile could be determined. Since a maximum speed is imposed, the lateral acceleration is also lowered for some parts of the prescribed path and the tyres have the capacity to generate forces in the longitudinal direction.

Since the tyres are now able to generate forces in the longitudinal direction, the vehicle can accelerate and decelerate. This acceleration and deceleration is limited either by the vehicle's performance capabilities or by the friction available for longitudinal force generation. By defining a preview distance and finding the minimum speed (as limited by the lateral acceleration) in the preview section, the inputs to the vehicle – accelerating or braking – may be determined and hence the vehicle speed calculated by assuming constant acceleration for a small interval. This results in the calculated speed profile. This speed profile is then used as the reference speed which the vehicle must attempt to track as it negotiates the prescribed path.

Before implementing the speed profile algorithm on the actual test vehicle, its performance was first tested on the MSC.ADAMS/View model of the Land Rover test vehicle (which was developed in Chapter 2). To track the reference speed profile, a PID controller was used for the throttle pedal actuation and a PI controller for the brake pedal actuation.

Simulation results indicate that the vehicle performs as planned, tracking the reference speed profile closely (considering the slow dynamics of a vehicle such as a Land Rover Defender) and

that the accelerations measured largely stay within the friction circle. The instances where the lateral acceleration exceeds the set limit are attributable to path following errors. During all of these simulations, the maximum permissible lateral and longitudinal accelerations were set to 8 m/s^2, which are very high limits for any road vehicle, especially a sports-utility-vehicle. Throughout the simulation, the steering controller developed by Botha (2011) maintained control over the vehicle. Hence the development of the longitudinal control system was deemed to have been successful. The next step in the process is experimental validation of the control systems.

Chapter 4

Experimental validation

Today's scientists have substituted mathematics for experiments, and they wander off through equation after equation, and eventually build a structure which has no relation to reality

–Nikola Tesla (1856-1943) Serbian-American engineer, physicist and inventor

4.1 Introduction

The performance of the control system developed in Chapter 3 will be evaluated by conducting field tests. During field testing, external inputs due to wind loading, gradients, varying friction and other dynamic effects that are not captured by the simulations may influence the performance of the control system negatively. The ability of the control system to overcome these external influences or disturbances gives an idea of the robustness of the system. The aim of the experimental validation is to investigate whether the developed control system will be able to reduce the vehicle's speed before performing a severe double lane change manoeuvre (ISO 3888-1:1999) so that the vehicle's lateral and longitudinal acceleration stays within prescribed boundaries.

4.2 Experimental setup

The Land Rover Defender test vehicle was used as the platform to validate the longitudinal control system developed in Chapter 2 and simulated in Chapter 3.

4.2.1 Actuators

The pneumatic actuator that controls the vehicle's brakes, as developed by Mathebula (2009), experienced difficulties with air supply. This was addressed by upgrading the air reservoir used. Figure 4.1 shows the upgraded air supply system and valve box that contains the proportional and on/off valves, a schematic diagram showing the valve layout is given in Figure 4.2. Furthermore, the fuzzy logic approach used by Mathebula (2009) was modified to PID control using the brake line hydraulic pressure as feedback. Figure 4.3 shows the brake actuator performance for ramp and parabolic desired pressures. It may be seen in Figure 4.3 that the

measured pressure closely follows the prescribed pressure, thus the control system is well-tuned. Other actuators as described in Chapter 2 did not require modifications or were not used.

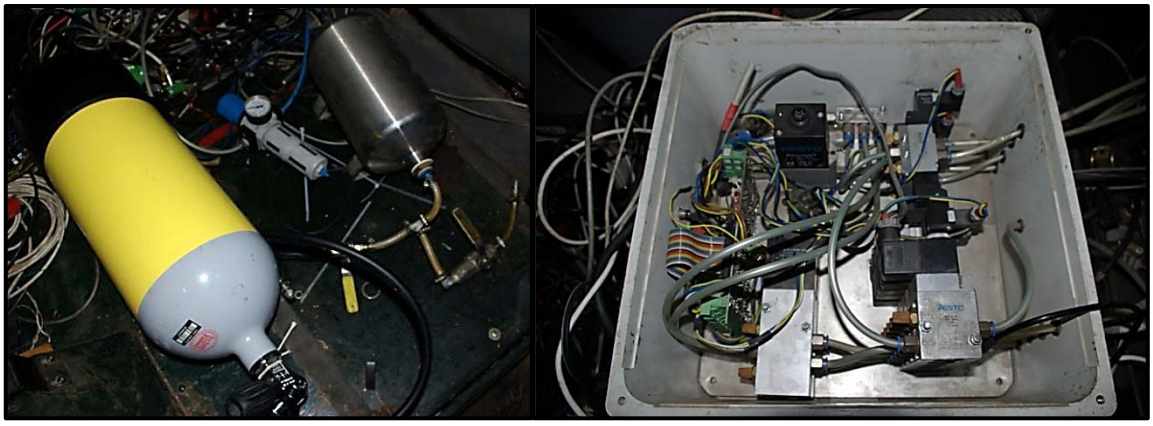

Figure 4.1 – Brake actuator setup showing air supply (left) and valve box (right)

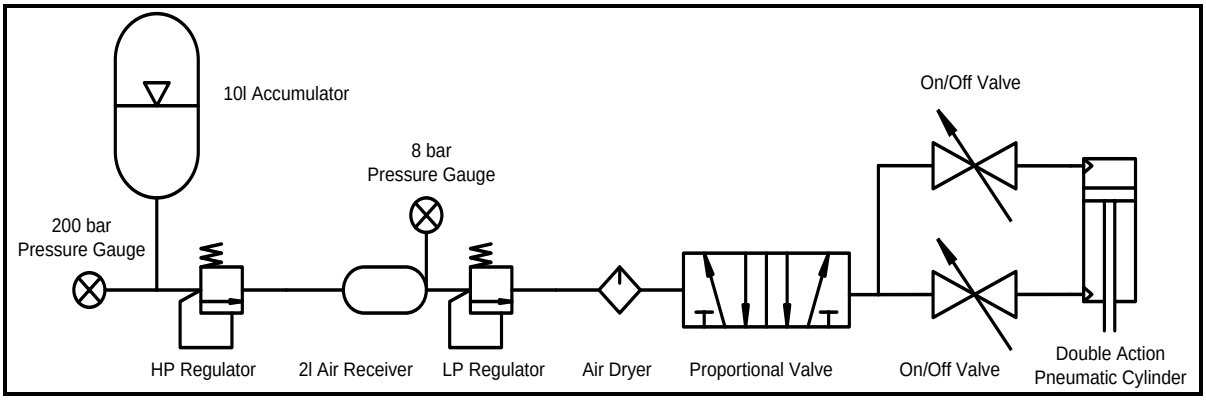

Figure 4.2 – Schematic showing valve layout

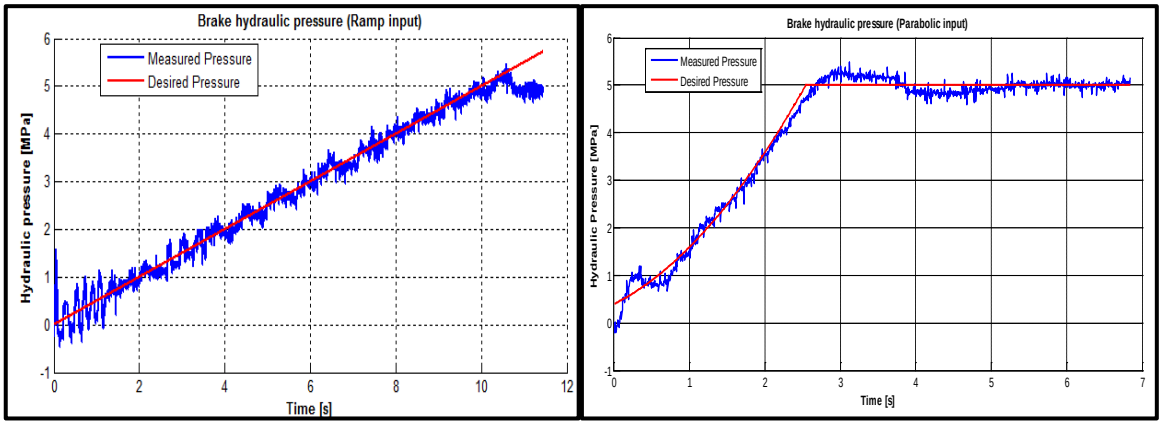

Figure 4.3 – Brake actuator response to ramp (left) and parabolic (right) inputs

4.2.2 Data acquisition and control system

The measurement transducers used during the experimental validation were:

- An accelerometer at the centre of gravity (CG) of the test vehicle to measure longitudinal and lateral acceleration
- A VBox III Differential GPS (Racelogic 2008) to measure the vehicle's speed and GPS position
- A hydraulic pressure transducer to measure the brake line hydraulic pressure
- A rotary potentiometer to measure the throttle position.

A PC/104 form factor embedded computer with a Diamond MM-AT-12-bit Analogue to Digital I/O Module was used for data acquisition. Since the longitudinal control is a very slow dynamic process, a sample frequency of 100Hz was deemed sufficient for both data acquisition and control.

The VBox III Differential GPS (Racelogic 2008) is a data logging system that can log GPS data at 100Hz. A Local Differential GPS Base station was used in conjunction with the VBox III to improve the positional accuracy to within 100mm. The same system was used by Botha (2011) as positional input to his steering controller with resounding success.

A laptop, connected to the PC/104 computer via a TCP network, was used in conjunction with the PC/104 to obtain the GPS coordinates and vehicle speed from the VBox III. The measured velocity and prescribed velocity were compared and a velocity error calculated. The velocity error was used to determine whether the brakes had to be applied or not. The PC/104 computer was used to control the actuators, generating an analogue output to control the brake line pressure. A corresponding prompt was given to the driver as an indication whether the brakes were going to be applied or not.

4.3 Experimental procedure

For the purpose of experimental validation, a severe double lane change manoeuvre (ISO 3888-1:1999) was performed. The boundaries of the severe double lane change were laid out with high visibility cones. The experimental procedure may be described as follows:

1. Record the path to be driven by driving at low speed.
2. Define the lateral and longitudinal acceleration boundaries.
3. Calculate the speed profile, as discussed in Chapter 3.
4. Perform a severe double lane change manoeuvre (ISO 3888-1:1999).

The GPS coordinates of the path to be driven are recorded with the VBox III. These GPS coordinates are converted to *x* and *y* coordinates (shown in Figure 4.4) that are then used to determine the speed profile (see Figure (3.2) for a schematic on determining the speed profile). The speed profile is determined as a function of GPS position.

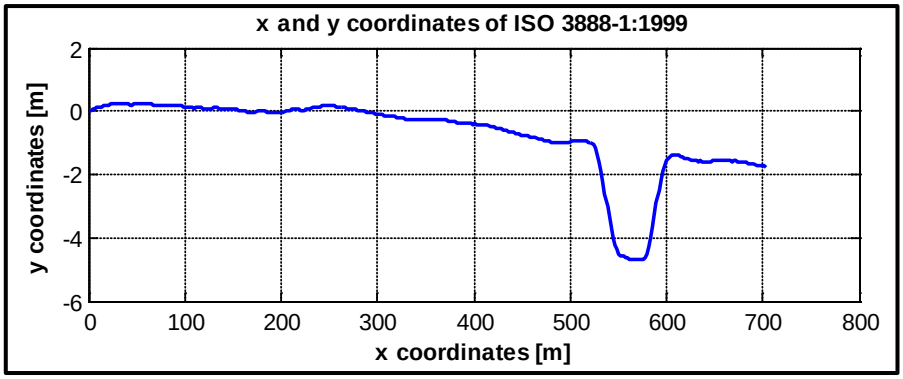

Figure 4. 4 – Recorded x and y coordinates of ISO 3888-1:1999 severe double lane change

While negotiating the severe double lane change, the vehicle compares its current speed (as measured with the VBox III) with the prescribed speed at that position. If the measured speed is below the prescribed speed, the vehicle is allowed to accelerate. The vehicle's brakes are applied if the measured speed is above the prescribed speed.

The only actuator used for experimental validation was the pneumatic actuator that controls the vehicle's deceleration by braking. The driver manually operated the throttle, clutch, gears and steering during the validation run. The reason for this is that the control system developed by Barnard (2008b) to control the clutch release was not smooth enough for safe operation during the tests. However, the application of the brakes to prevent the driver from exceeding the lateral acceleration limits of the vehicle was deemed to be sufficient for validation. During the run a prompt was displayed on a computer screen indicating whether the vehicle's speed was too high or too low. If the brakes were being applied, the driver disengaged the clutch. This was to prevent the vehicle from stalling while performing the double lane change manoeuvre (this may happen if the engine speed drops below idle speed due to the vehicle driving too slow for the selected gear). Figure 4.5 shows the Land Rover as it is about to enter the double lane change manoeuvre. Note that the brake lights are on.

Figure 4.5 – The Land Rover braking prior to entering the double lane change

4.4 Experimental results

The results obtained from the experimental procedure outlined in Section 4.3 are plotted in Figures 4.6 to 4.10. Each plot contains five graphs, namely:

- The *x* and *y* coordinates of the path followed during the test run in the top left corner.
- A g-g diagram showing lateral and longitudinal acceleration during the run. Included in the g-g diagram are red friction circles for incrementing longitudinal and lateral acceleration, i.e. the innermost circle is for $1m/s^2$ lateral and longitudinal acceleration, the second circle for $2m/s^2$ lateral and longitudinal acceleration and so forth.
- The graph second from the top is a plot of the measured vehicle speed (blue) and the prescribed vehicle speed (red).
- The third graph from the top shows the desired brake line pressure (red) and the measured brake line pressure (blue).
- The bottom graph plots lateral (red) and longitudinal acceleration (blue) as functions of the distance travelled from the starting point.

The double lane change manoeuvre was performed at various prescribed lateral and longitudinal acceleration limits. Initially, the prescribed longitudinal acceleration limit was set to $6m/s^2$ and $8m/s^2$ while doing multiple double lane change manoeuvres at various prescribed lateral acceleration limits. The prescribed longitudinal acceleration limit was then reduced to $3m/s^2$, a value more readily associated with everyday driving. Finally, the validation run was done with a low prescribed longitudinal acceleration limit of $1m/s^2$.

4.4.1 DLC at $3m/s^2$ lateral and $8m/s^2$ longitudinal acceleration

In Figure 4.6, the results of a double lane change with prescribed limits of $3m/s^2$ lateral and $8m/s^2$ longitudinal acceleration respectively are plotted. During this manoeuvre maximum longitudinal acceleration of $4m/s^2$ and lateral acceleration of $3m/s^2$ were recorded, while negotiating the double lane change at approximately 10m/s. The driver managed to fully disengage the clutch during the manoeuvre and as a result the vehicle closely tracked the prescribed speed and hence the lateral acceleration stayed within the prescribed limit. The brake actuator closely followed the desired pressure, indicating that the PID control used for brake actuation operated as expected.

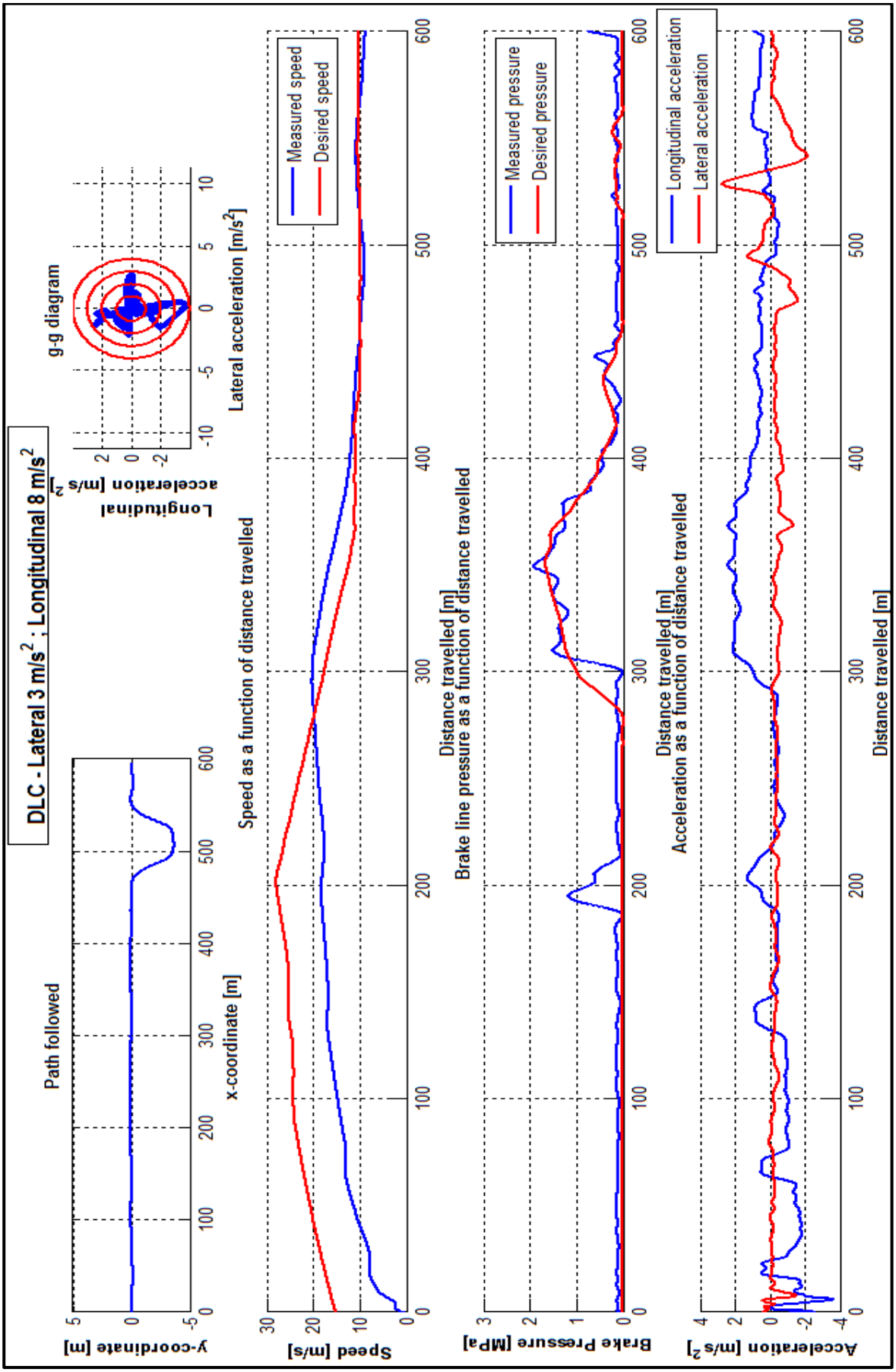

Figure 4.6 – Double lane change with lateral and longitudinal limits of 3m/s^2 and 8m/s^2 respectively

4.4.2 DLC at 5m/s² lateral and 8m/s² longitudinal acceleration

The results of the double lane change manoeuvre with prescribed acceleration limits of 5m/s^2 lateral and 8m/s^2 longitudinal acceleration are shown in Figure 4.7. A vehicle speed of approximately 13m/s was maintained during the double lane change manoeuvre, resulting in a maximum lateral acceleration of 3.5m/s^2. The maximum longitudinal acceleration recorded during the manoeuvre was 3m/s^2. The control system managed to accurately track the desired brake line pressure and hence the speed during the double lane change was very close to the prescribed speed and the acceleration in both the longitudinal and lateral directions stayed well within the prescribed limits.

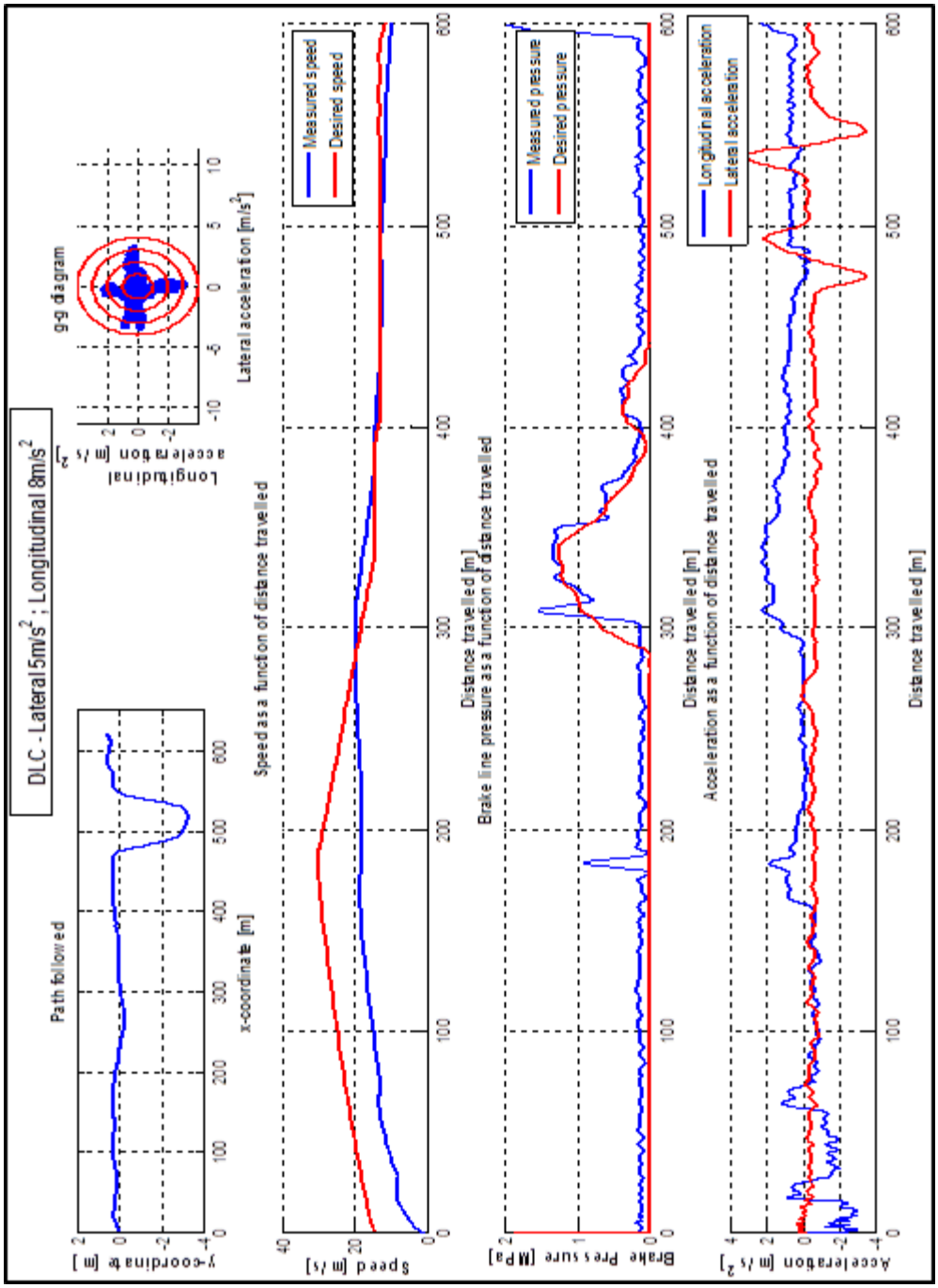

Figure 4.7 – Double lane change with lateral and longitudinal limits of 5m/s^2 and 8m/s^2 respectively

4.4.3 DLC at 7m/s² lateral and 8m/s² longitudinal acceleration

The highest prescribed lateral acceleration limit tested at was 7m/s^2 and the results thereof are shown in Figure 4.8. The maximum lateral and longitudinal accelerations measured during the double lane change manoeuvre were 4m/s^2 and 3.2m/s^2 respectively, well within the prescribed limits. The double lane change was negotiated at 14m/s, slightly lower than the speed as prescribed by the speed profile algorithm and hence the lateral acceleration was significantly lower than the prescribed limit. The actuator applying the brakes accurately tracked the desired brake line pressure, but the vehicle lost too much speed. This may be attributed to driver error, the driver neglecting to maintain the speed once the double lane change had been entered.

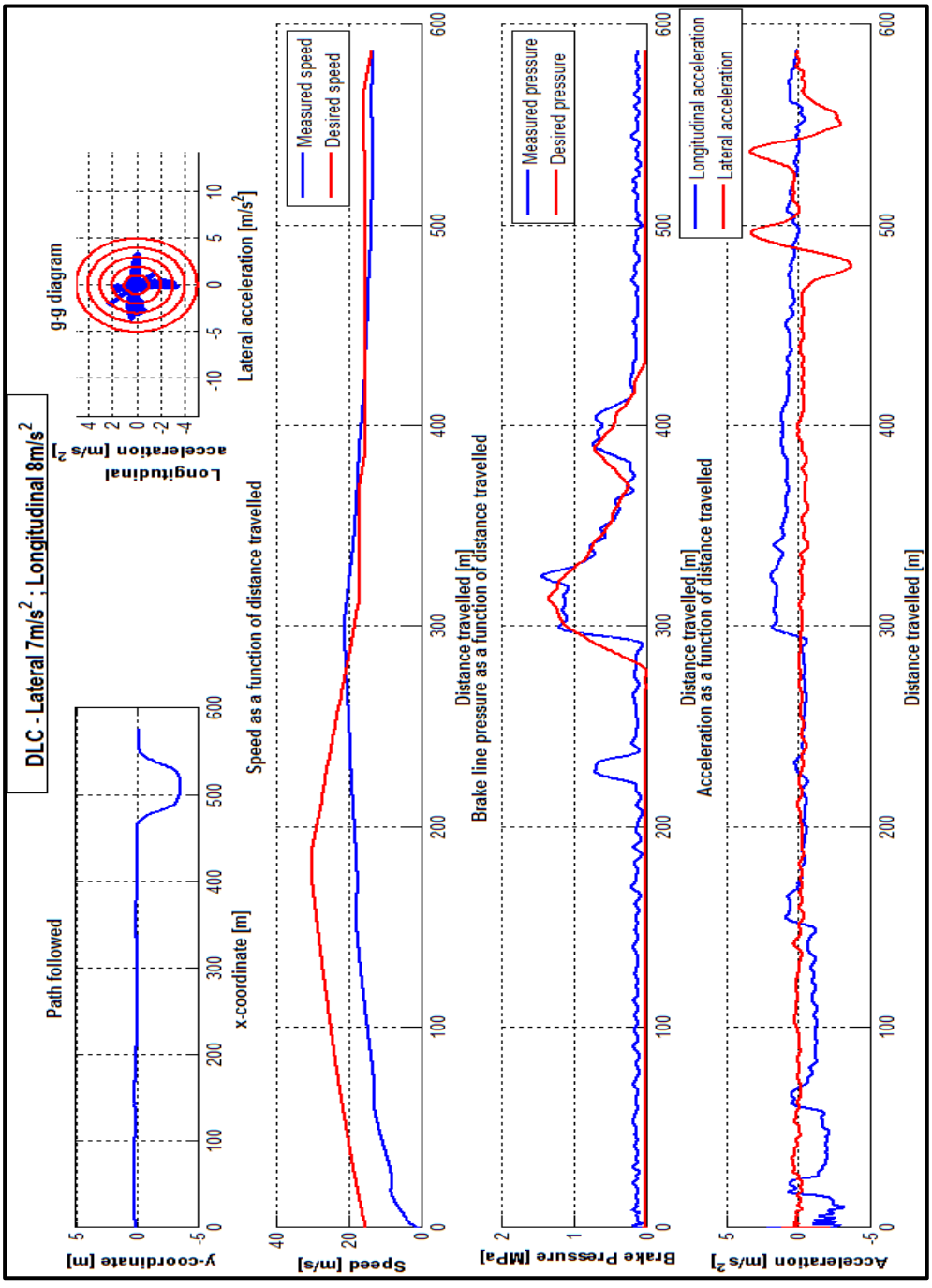

Figure 4.8 – Double lane change with lateral and longitudinal limits of 7m/s^2 and 8m/s^2 respectively

4.4.4 DLC at 3m/s² lateral and 3m/s² longitudinal acceleration

The prescribed longitudinal acceleration limit was reduced to 3m/s^2, with the lateral acceleration limit at 3m/s^2 and the experimental results are shown in Figure 4.9. The reason for the low prescribed lateral acceleration limit is because the low prescribed longitudinal acceleration limit prevented the Land Rover from reaching a speed high enough to excite high lateral accelerations. During the double lane change, the maximum lateral acceleration measured was 2.8m/s^2 and the maximum longitudinal acceleration 2m/s^2, the vehicle thus stayed within the prescribed acceleration limits. The double lane change was negotiated at 10m/s, similar to the speed in Section 4.4.2 which has the same prescribed lateral limit.

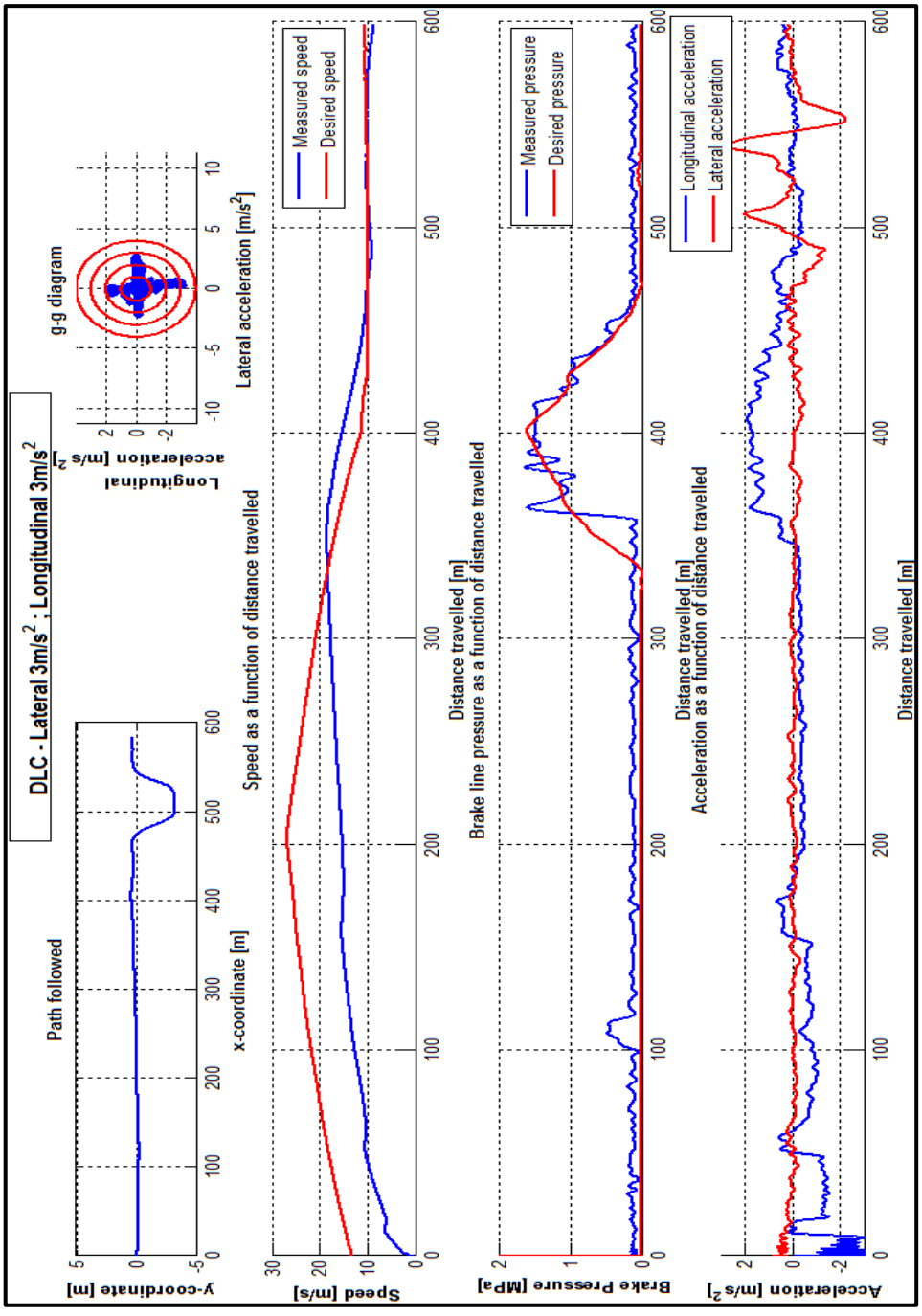

Figure 4.9 – Double lane change with lateral and longitudinal limits of 3m/s^2 and 3m/s^2 respectively

4.4.5 DLC at 3m/s² lateral and 1m/s² longitudinal acceleration

The last double lane change manoeuvre was performed with 3m/s^2 and 1m/s^2 as the prescribed lateral and longitudinal acceleration limits and the results are shown in Figure 4.10. During the double lane change manoeuvre, the vehicle tracked the prescribed speed accurately, resulting in maximum measured lateral and longitudinal accelerations of 2.3m/s^2 and 0.93m/s^2 respectively. The accelerations measured were thus within the prescribed limits. Very little brake actuation was present, the vehicle decelerating mainly due aerodynamic drag and rolling resistance.

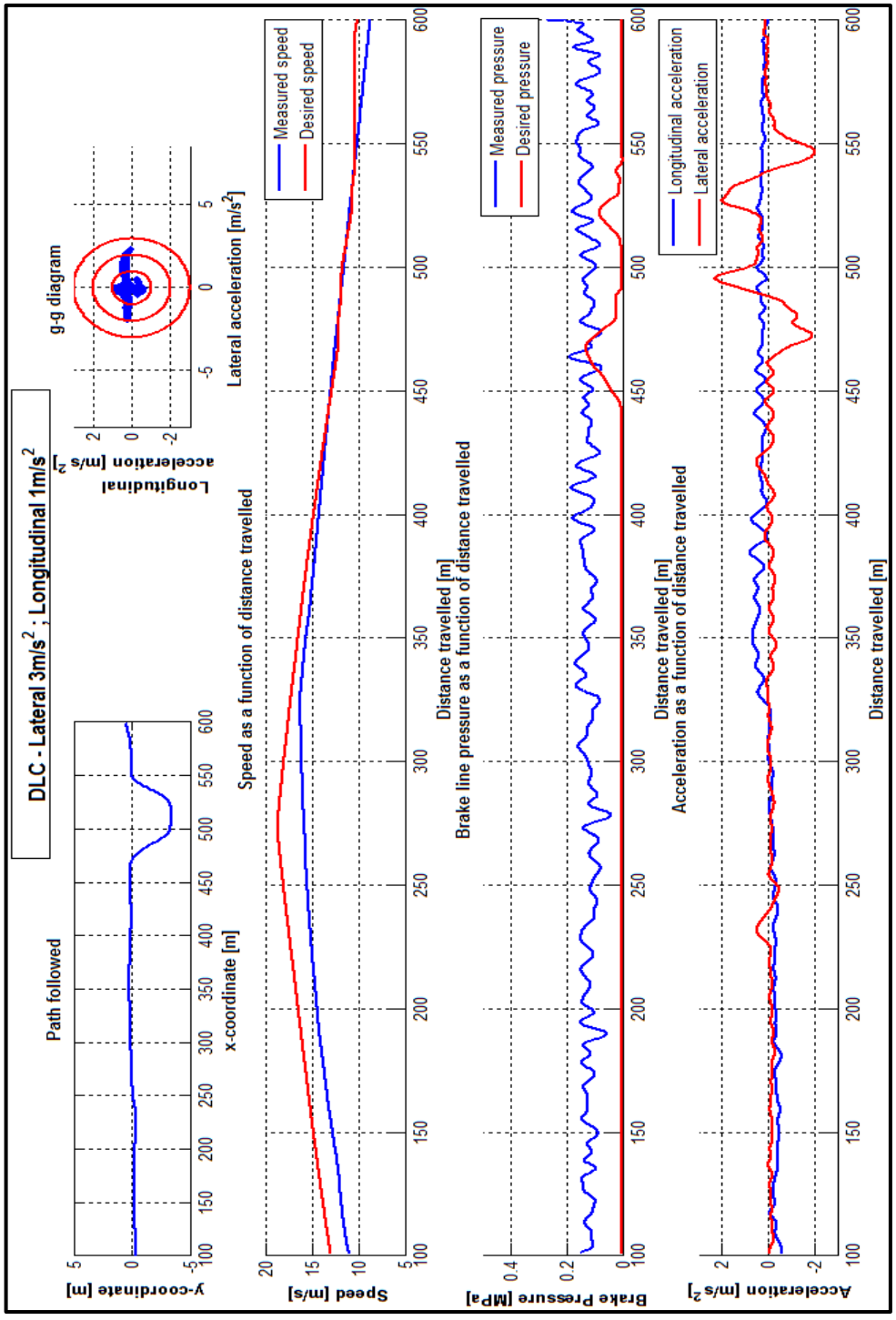

Figure 4.10 – Double lane change with lateral and longitudinal limits of 3m/s^2 and 1m/s^2 respectively

4.5 Discussion of results

During all of the double lane change manoeuvres performed the lateral acceleration of the vehicle was reduced as desired by controlling the longitudinal behaviour of the vehicle. In all of the tests, the measured accelerations never exceeded the prescribed boundaries. The vehicle reduced speed when it exceeded the prescribed speed, resulting in the measured accelerations being within the desired boundaries.

The pneumatic actuator used to control the vehicle's brakes accurately tracked the desired brake line pressure in all of the tests, even when noise was present. This validated the design of the PID controller used to control the brake line pressure.

The prescribed longitudinal acceleration limit was only reached when the prescribed limit was low. When the prescribed longitudinal acceleration was high, the vehicle braked early, resulting in lower longitudinal accelerations being measured. A possible explanation for this is that the preview distance used to determine when to apply the brakes is too conservative, effectively looking too far ahead when the prescribed longitudinal acceleration is high.

4.6 Conclusion

The performance of the speed profile algorithm developed in Chapter 3 was tested by performing severe double lane change manoeuvres for varying prescribed longitudinal and lateral accelerations. The speed profile algorithm was used to determine a reference speed that the Land Rover test vehicle had to maintain while approaching and negotiating the double lane change manoeuvre.

The air supply problem experienced by the pneumatic actuator used to control the brake line pressure of the Land Rover test vehicle was addressed by integrating a 10l, 20MPa air reservoir. The control system used to control the brake line pressure was modified from fuzzy logic to PID control so that better control over the actuator was obtained. The upgraded pneumatic actuator was tested under laboratory and field conditions and performed adequately.

An experimental procedure to validate the speed profile algorithm was developed and numerous tests were performed at the Gerotek Test Facilities. During the tests the pneumatic brake actuator was used to limit the vehicle's speed while negotiating the severe double lane change manoeuvre, while measuring the longitudinal and lateral acceleration of the vehicle. The measured accelerations stayed within the prescribed boundaries, with the longitudinal acceleration never reaching the prescribed boundary. This indicates that the speed profile algorithm developed is conservative in determining when to apply the brakes, braking too early rather than too late. The reason for the system being conservative is to add robustness to the speed profile algorithm, allowing it to be used for any prescribed acceleration boundaries. In this case, being conservative is a better approach to being reckless, because the safety of the vehicle's occupants is at stake.

Multiple improvements to the system are possible. Adding the steering controller (developed by Botha (2011)) and developing a control system that uses the existing pneumatic actuator to smoothly operate the vehicle's clutch will allow the vehicle to be operated fully autonomously. By operating the vehicle autonomously, the desired speed and the prescribed path, as formulated with the trajectory planning algorithm of Chapter 3, may be tracked more accurately which in turn should yield improved field results.

Furthermore, the trajectory may be optimised in real time. By optimising the trajectory in real time, a more accurate speed profile that takes into account the vehicle's current position (including the error) may be formulated. This may result in reducing the lateral acceleration of the vehicle even more.

In conclusion, the experimental results indicate that the application of the speed profile algorithm to limit the vehicle's speed results in reduced lateral accelerations. This is in agreement with the simulation results discussed in Chapter 3. It is thus safe to say that the speed profile algorithm has been experimentally validated to reduce the lateral accelerations to prescribed limits by limiting the vehicle's speed prior to entering a severe manoeuvre. Further validation may be done by investigating the control system's performance when negotiating a racetrack or a test track similar to public roads.

Chapter 5

Conclusion and recommendations

I think and think for months and years. Ninety-nine times, the conclusion is false. The hundredth time I am right – Albert Einstein (1879-1955) German physicist

5.1 Conclusion

This study set out to develop a control system that prevents a vehicle from exceeding its lateral limitations. Control systems are being implemented as driver aids in commercial vehicles and several projects worldwide are aimed at developing fully autonomous vehicles, but the focus of these projects are aimed mainly at developing the artificial intelligence of the vehicle and usually neglect, simplify or linearize the multi-body vehicle dynamics. The goal for this project was to develop a control system that is based on a highly non-linear multi-body dynamics full-vehicle model (a model-based-design approach). The control system was aimed at improving the safety of a sports-utility-vehicle by limiting the vehicle's speed or increasing the radius of curvature of the path being followed (through optimising the trajectory) to reduce the lateral acceleration experienced by the vehicle.

A Land Rover Defender 110 Wagon was the vehicle used as implementation platform for the developed control system. At the University of Pretoria, several projects have been aimed at developing actuators and control systems that can be used autonomously. Simultaneously, an experimentally validated model of the Land Rover Defender was developed in MSC.ADAMS/View that accurately captures the lateral and vertical dynamics. The MSC.ADAMS/View model was expanded to accurately include:

- the engine map
- the demand forces acting on the vehicle
- the longitudinal deceleration of the vehicle when applying the brakes and
- the engine braking torque.

These longitudinal characteristics of the Land Rover Defender were validated experimentally by performing a validation test run and measuring the inputs given by the driver and the resulting vehicle speed. The measured driver inputs were given to the model of the Land Rover in MSC.ADAMS/View and the simulated speed compared with the measured vehicle speed. The correlation between the measured and simulated speed was deemed adequate.

A longitudinal control system was developed to reduce the vehicle's lateral acceleration by maximising turn radius and limiting speed. The trajectory of the track or road to be followed was optimised to maximise the radius of the path to be followed. This optimised trajectory was used in conjunction with a driver model to define a speed limit for the vehicle at each point on the trajectory. The driver model took into account prescribed longitudinal and lateral acceleration limits and the vehicle's lateral acceleration limits, the friction available for combined longitudinal and lateral force generation (due to the friction circle concept) and the vehicle's longitudinal performance capabilities to formulate a safe speed at each point of the path being followed. The process of optimising the trajectory and determining a safe speed was termed the speed profile algorithm.

The performance of the longitudinal control system was evaluated using the validated MSC.ADAMS/View model of the Land Rover Defender. Several racetracks of which the GPS coordinates are available were used for simulation purposes. A speed profile was developed for each racetrack and MSC.ADAMS/View was used in conjunction with MATLAB and Simulink to simulate the Land Rover Defender negotiating these tracks. In all of the simulations, the steering controller maintained control over the vehicle, even though the model was operating very close to the vehicle's limits. Throughout the simulations, the lateral and longitudinal accelerations stayed within the prescribed limits. The simulation results indicated that the longitudinal control system was safe for experimental validation on the Land Rover Defender.

Experimental validation of the longitudinal control system was done by performing an ISO 3888-1:1999 severe double lane change manoeuvre. Speed profiles for the double lane change were formulated with various prescribed longitudinal and lateral acceleration limits. The pneumatic actuator used for controlling the brake line pressure was used to prevent the vehicle from exceeding the speed deemed safe by the speed profile algorithm. During all the test runs, the vehicle's measured lateral and longitudinal accelerations were within the prescribed limits. The system was found to be conservative, rarely reaching the prescribed longitudinal acceleration. The reason for the system being conservative is to add robustness to the speed profile algorithm, allowing it to be used for any prescribed acceleration limits.

5.2 Recommendations

Multiple aspects which could improve the longitudinal control system and speed profile algorithm at higher prescribed acceleration limits have been identified. These include:

- Investigating the control system's performance when negotiating a racetrack or a test track that resembles typical public roads. Such an investigation may lead to further improvements in the control system and may result in the control system not being so conservative.

- Development of a control system that smoothly engages the vehicle's clutch. Such a control system must allow the vehicle to pull away and change gears autonomously. Furthermore, when the brakes are applied, the clutch must be disengaged.

- Fixing the steering robot developed by Botha (2011). By fixing the steering robot, the vehicle may be operated autonomously. This will enable the vehicle to follow the optimised trajectory by relying on GPS position rather than the human driver.

- The development of software that can optimise the trajectory in real time, taking account of the vehicle's current position, may result in a safer speed limit being formulated.

- Additional sensors that may detect and can hence be used to avoid obstacles or lane departure warning systems may be integrated with the system. This may result in a more fully autonomous vehicle.

- By incorporating all the driver aids developed on the Land Rover Defender at the University of Pretoria, significant improvements in vehicle safety may be achieved. A strategy to decide when to employ which driver aid will need to be developed.

- The Land Rover Defender is to some extent an out dated platform. Implementing the autonomous control systems developed for the Land Rover Defender on a modern vehicle which uses drive-by-wire technology may also result in quicker actuator response and hence improved vehicle performance.

Performing these recommendations may result in significant improvements in the vehicle's performance, safety and stability.

References

Abe, M. 2009. *Vehicle Handling Dynamics – Theory and Application.* Butterworth-Heinemann, Oxford, UK.

Bakker, E., Pacejka, H.B., Lidner, L. 1989. 'A New Tire Model with an Application in Vehicle Dynamics Studies', SAE Technical Paper 890087. Society of Automotive Engineers, Inc.

Barnard, C.J. 2008a. *Design of Automated Gear-shift and Clutch Control.* BEng(Mechanical) Final year design, University of Pretoria.

Barnard, C.J. 2008b. *Design of an Automated Gear-shift and Clutch Controller.* BEng(Mechanical) Final year project, University of Pretoria.

Binsfeld Engineering Inc. *TorqueTrak 9000 Digital Telemetry System Users Manual*. Binsfeld Engineering Inc, Maple City, MI. Available online at: www.binsfeld.com

Blundell, M. and Harty, D. 2004. *The Multibody Systems Approach to Vehicle Dynamics.* Butterworth-Heinemann, Oxford, UK.

Botha, T.R. 2008. *Brake Control – Autonomous Vehicle Brake System.* BEng(Mechanical) Final year project, University of Pretoria.

Botha, T.R. 2011. *High Speed Autonomous Off-Road Vehicle Steering*. MEng(Mechanical) Thesis, University of Pretoria, available online: http://upetd.up.ac.za/thesis/available/etd-11212011-125411/

Botha, T.R. and Els, P.S. 2011. 'High Speed Autonomous Off-road Vehicle Steering' published in the proceedings of the *17th International Conference of the International Society for Terrain-Vehicle Systems,* September 18-22, 2011, Blacksburg, Virginia, USA.

Braghin, F., Melzi, S., Sabbioni, E. and Poerio, N. 2011. 'Identification of the optimal trajectory for a race driver', *Proceedings of the ASME 2011 International Design Engineering Technical Conferences & Computers and Information in Engineering Conference.* 28-31 August 2011. American Society of Mechanical Engineers, Washington DC, USA.

Burden, R.L. and Faires, J.D. 2005. *Numerical Analysis – Eighth Edition.* Thomson Brooks/Cole, Belmont, CA.

Cronje, P.H. 2008. *Improving Off-Road Vehicle Handling Using an active Anti-Roll Bar*. MEng(Mechanical) Thesis, University of Pretoria, available online: http://upetd.up.ac.za/thesis/available/etd-11262009-011206/

DARPA. 2008. *Urban Challenge Overview*. Viewed 11 January 2012: http://archive.darpa.mil/grandchallenge/overview.asp

Diamond Systems Corporation. 2004. *DIAMOND-MM-AT User Manual V1.21.* Diamond Systems Corporation, Newark, CA.

Dorf, R.C. and Bishop, R.H. 2008. *Modern Control Systems – Eleventh Edition.* Pearson Prentice Hall, Upper Saddle River, NJ.

Gerotek Test Facilities, available online at http://www.armscordi.com/SubSites/Gerotek1/Gerotek01_landing.asp

Gillespie, T.D. 1992. *Fundamentals of Vehicle Dynamics.* Society of Automotive Engineers, Warrendale, PA.

Goldsmith, T.C. 1998. *Automated Vehicle Guidance (AVCS) – The Real Automobile.* Viewed 11 January 2012: http://www.azinet.com/articles/real98.htm

Hamersma, H.A. 2011. *Longitudinal Vehicle Dynamics Model*. B.Eng(Hons) (Mechanical) Independent Study Report, University of Pretoria.

Hoedemaeker, M. and Brookhuis, K.A. 1998. 'Behavioural adaptation to driving with an adaptive cruise control (ACC)', *Transportation Research Part F: Traffic Psychology and Behaviour.* Vol. 1, Issue 2, December 1998. Viewed on 2 April 2013: http://www.sciencedirect.com/science/article/pii/S1369847898000084

International Organization for Standardization. 1999. *Passenger cars – Test track for a severe lane-change manoeuvre – Part 1: Double lane-change (*ISO 3888-1:1999), SAI Global Database.

Ioannou, P.A. and Chien, C.C. 1993. 'Autonomous Intelligent Cruise Control', *IEEE Transactions on Vehicular Technology*. Vol. 42, No. 4, pp. 657-671.

Jazar, R.N. 2008. *Vehicle Dynamics: Theory and Applications.* Springer Science+Business Media, New York, NY.

MacAdam, C.C. 2003. 'Understanding and Modeling the Human Driver', *Vehicle System Dynamics*. Vol. 40, Nos. 1-3, pp. 101-134.

Mathebula, I.S. 2009. *Autonomous Land Rover Defender Project – Brake pedal control.* BEng(Mechanical) Final year project, University of Pretoria.

Meriam, J.L. and Kraige, L.G. 2003. *Engineering Mechanics Dynamics – Fifth Edition.* John Wiley & Sons, Hoboken, NJ.

Montemerlo, M., Thrun, S., Dahlkamp, H., Stavens, D. and Strohband, S. 2006. 'Winning the DARPA Grand Challenge with an AI Robot', *Proceedings of the Twenty-First AAAI Conference on*

Artificial Intelligence. 16-20 July 2006. Association for the Advancement of Artificial Intelligence, Boston, MA.

Peden M.M., Krug E., Mohan D., Hyder A., Norton, R., MacKay, M., and Dora, C. 2002. Five-year WHO Strategy on Road Traffic Injury Prevention. Geneva: World Health Organization, Ref : WHO/NMH/VIP/01.03

Plöchl, M. and Edelmann, J. 2007. 'Driver models in automobile dynamics application', *Vehicle System Dynamics: International Journal of Vehicle Mechanics and Mobility*. Vol. 45:7-8, pp. 699-741.

Racelogic. 2008. *VBOXTools Software Manual ver1.9.* Viewed on 12 March 2013: http://www.racelogic.co.uk/_downloads/vbox/Manuals/Data_Loggers/RLVB3_Manual%20-%20English.pdf

Rao, S.S. 2009. *Engineering Optimization Theory and Practice – Fourth Editon.* John Wiley & Sons, Hoboken, NJ.

Rover Group Limited. 1996. *Workshop manual Defender 300Tdi.* Rover Technical Corporation, London.

Stewart, J. 2003. *Calculus Early Transcendentals – Fifth Edition.* Brooks/Cole – Thomson Learning, Belmont, CA.

'Tech Inside: Autonomous Emergency Braking'. 2012. *Popular Mechanics South Africa*. Viewed on 7 March 2013: http://www.popularmechanics.co.za/wheels/tech-inside-autonomous-emergency-braking/

Technology Talks. 2010. *Google Car Road Test: Google Car Drives without Human Driver.* Viewed on 6 March 2013: http://www.kokeytechnology.com/cars-and-auto-parts/0963-google-car-road-test-google-car-drives-without-human-driver/

Thoresson, M.J. 2007. *Effcient Gradient-Based Optimisation of Suspension Characteristics for an Off-Road Vehicle*. PhD(Mechanical Engineering) thesis, University of Pretoria, available online: http://upetd.up.ac.za/thesis/available/etd-08042008-093103/

Uys, P.E., Els, P.S. and Thoresson, M.J. 2007. 'Suspension settings for optimal ride comfort of off-road vehicles travelling on roads with different roughness and speeds', *Journal of Terramechanics*. Vol. 44, pp. 163-175.

Vestri, C., Bougnoux,S., Bendahan, R., Fintzel, K., Wybo, S., Abad, F. and Kakinami, T. 2005. 'Evaluation of a Vision-Based Parking Assistance System', *Proceedings of the 8th International IEEE Conference on Intelligent Transportation Systems.* 13-16 September 2005, Vienna, Austria.